cases of $CD5^-CD10^-$). Three $CD5^+$ cases possessed $CD10^+$. Informed consent was provided according to the Declaration of Helsinki. It should be noted that we especially collected a total of 36 cases of $CD5^+$ DLBCL, which represent a higher ratio than that found in the standard population, for evaluation of the genetic status of this disease entity. We analyzed genomic imbalances for the 99 cases of DLBCL by use of array CGH. Forty-six of these cases (22 cases of $CD5^+$, 7 cases of $CD5^-CD10^+$, and 17 cases of $CD5^-CD10^-$) were subsequently subjected to gene-expression profiling. In addition, none of the patients had a previous history of malignant lymphoma. All the DNA and RNA samples were obtained from tumors at the time of diagnosis before any treatment was administered, while all the patients with DLBCL received adequate doses of a cyclophosphamide, Adriamycin, vincristine, and prednisone (CHOP)–like regimen after diagnosis. All patients' data regarding age, stage, performance status, lactate dehydrogenase (LDH) level, number of extranodal sites, and International Prognostic Index (IPI) score at diagnosis are shown in Table 1.

Gene-expression profiling

Total RNA was isolated from each specimen by means of cesium chloride centrifugation. Cyanine 5 (Cy5)– or Cy3-labeled complementary RNA (cRNA) was generated from total RNA by using a Low RNA Input Linear Amplification Kit (Agilent Technologies, Palo Alto, CA). Probes consisted of a mixture of an experimental Cy5-labeled cRNA and control Cy3-labeled cRNA. The latter was prepared from a pool of total RNA from 10 hyperplasia lymph node samples. The microarray glass slide consisted of an Agilent oligonucleotide array custom-made for the Cancer Institute of the Japanese Foundation for Cancer Research, on which a total of 21 619 genes were spotted (Agilent Technologies). Probes were hybridized overnight on the glass slides with an In Situ Hybridization Kit Plus (Agilent Technologies) according to the manufacturer's protocol. Fluorescent images of hybridized microarrays were obtained with an Agilent scanner G2565AA (Agilent Technologies), which were then analyzed with Feature Extraction software (Agilent Technologies) to obtain the ratios of the fluorescence of the experimental Cy5-labeled samples to that of the Cy3-labeled control. All nonflagged fluorescence ratios were log-transformed (base 2) and centered by subtracting the median observed value of each gene determined by cluster analysis. The hierarchical clustering algorithm was applied to DLBCL cases according to the expression level of these genes with the aid of Cluster and TreeView software (Eisen Lab, http://rana.lbl.gov/EisenSoftware.htm).[13] Of the 100 genes specified by Rosenwald et al[8] for clustering ABC and GCB groups, 67 of which were available to use for clustering analysis. These 67 genes are *BARD1, PIK3CG, LRMP,* Hs.1098, *BCL6, HDAC1, MYBL2, MME (CD10), STAG3, LMO2, APS,* Hs.151051, *ADPRT, ITPKB, REL, FLJ20094,* Hs.211563, *MEF2B, CD44,* Hs.75765, *IL6, PTPN2, PTPN12, BMI1,* Hs.128003, *BACH2, HIVEP1, CFLAR, APAF1, RYK, EDG1, KIAA0874,* Hs.153649, *MADH4, PTPN1,* Hs.93213, *DCTD,* Hs.193857, *IL16, SP140, SH3BP5, IRF4 (MUM1), TLK1, KCNA3, TCL1A, PAK1,* Hs.188, *CXCR4, SLA, CCND2, TGFBR2, ETV6, SPAP1, PM5, PDIR, IGHM, CD22,* Hs.296938, Hs.1565, Hs.83126, *MAPKAPK3, RUNX1,* Hs.55947, S100A4, *TFAP4, IRF2,* and *OPA1*. We performed clustering analysis with published microarray data by these 67 genes. DLBCL gene expression profile data generated by the Lymphochip microarrays were obtained from supplemental data of the article by Rosenwald et al.[8] We confirmed that the 274 DLBCL of the Lymphochip microarray data set could be divided into the ABC and the GCB and the Type 3 with these 67 genes. Distributions of tumors with aforementioned 67 genes were nearly identical to those with the 100 genes that were described by Rosenwald et al.[8]

Array CGH

Array CGH was performed for DLBCL cases by previously described methods using custom-made glass slide of Aichi Cancer Center (ACC) array slide version 4.0. The array consisted of 2304 BAC (Bacterial artificial chromosome) and PAC (P-1 derived artificial chromosome) clones (BAC/PAC clones), covering the whole human genome with roughly 1.3 Mb (megabase) of resolution. BAC clones were derived from RP11 and RP13 libraries, and PAC clones were derived from RP1, RP3, RP4, and RP5 libraries. BAC/PAC clones were subjected to degenerate oligonucleotide-primed polymerase chain reaction (PCR). The resulting DNA samples were

Table 1. Clinical features of DLBCL subgroups with distinct phenotypes and expressions

Characteristic	CGH analysis				Gene-expression profiling		
	$CD5^+$	$CD5^-CD10^+$	$CD5^-CD10^-$	Total	ABC	GCB	Total
Age							
Median, y (range)	62 (36-82)	65 (48-89)	57 (26-91)	60 (26-91)	67 (36-91)	63 (38-89)	64 (36-91)
No. patients*	36	19	44	99	28	18	46
Ann Arbor stage, no. patients (%)							
I-II	5 (15)	8 (42)	17 (49)	30	5 (20)	7 (41)	12
III-IV	29 (85)	11 (58)	18 (51)	58	20 (80)	10 (59)	30
Total*	34 (100)	19 (100)	35 (100)	88	25 (100)	17 (100)	42
Performance status, no. (%)							
0-1	24 (71)	16 (84)	30 (97)	70	16 (67)	16 (100)	32
2 or more	10 (29)	3 (16)	1 (3)	14	8 (33)	0 (0)	8
Total*	34 (100)	19 (100)	31 (100)	84	24 (100)	16 (100)	40
LDH level, no. patients (%)							
Normal	8 (24)	12 (63)	12 (38)	32	6 (25)	3 (19)	9
High	25 (76)	7 (37)	20 (62)	52	18 (75)	13 (81)	31
Total*	33 (100)	19 (100)	32 (100)	84	24 (100)	16 (100)	40
No. of extranodal sites, no. patients (%)							
1 or fewer	24 (73)	13 (68)	25 (78)	62	17 (71)	13 (81)	30
More than 1	9 (27)	6 (32)	7 (22)	22	7 (29)	3 (19)	10
Total*	33 (100)	19 (100)	32 (100)	84	24 (100)	16 (100)	40
IPI index, no. patients (%)							
L/LI	13 (38)	9 (47)	20 (65)	42	5 (19)	7 (41)	12
H/HI	21 (62)	10 (53)	11 (35)	42	21 (81)	10 (59)	31
Total*	34 (100)	19 (100)	31 (100)	84	26 (100)	17 (100)	43

Ninety-nine cases were subjected to array CGH analysis (left), and 46 of them to gene-expression profiling (right). L/LI, indicates low/low intermediate; H/HI, high/high intermediate.

*Number of patients whose clinical data were available.

robotically spotted by an inkjet technique (NGK, Nagoya, Japan) in duplicate onto CodeLink activated slides (Amersham Biosciences, Piscataway, NJ). BAC/PAC clones used were selected based on information from the National Center for Biotechnology Information (NIBC; http://www.ncbi.nlm.nih.gov/) and Ensembl Genome Data Resources (http://www.ensembl.org/). These clones were obtained from the BACPAC Resource Center at the Children's Hospital (Oakland Research Institute, Oakland, CA). DNA preparation, labeling, array fabrication, and hybridization were performed as described previously.[11,12]

For the array, 10 simultaneous hybridizations of healthy male versus normal male were performed to define the normal variation for the $\log_2$ ratio. A total of 91 clones with less than 10% of the mean fluorescence intensity of all the clones, with the most extreme average test over reference ratio deviations from 1.0 and with the largest SD in this set of normal controls was excluded from further analyses. Thus, we analyzed a total of 2213 clones (covered 2988 Mb, 1.3 Mb of resolution) for further analysis. Of the 2213 clones, 2158 (covered 2834 Mb) were from chromosome 1p telomere to 22q telomere; 55 of 2213 clones were from chromosome X.

Because greater than 96% of the measured fluorescence $\log_2$ ratio values of each spot (2 × 2191 clones) ranged from +0.2 to −0.2, the thresholds for the $\log_2$ ratio of gains and losses were set at the $\log_2$ ratio of +0.2 and −0.2, respectively. Regions of low-level gain were defined as $\log_2$ ratio +0.2 to +1.0, those suggested of containing a heterozygous loss/deletion as $\log_2$ ratio −1.0 to −0.2, those showing high-level gain as $\log_2$ ratio greater than +1.0, and those suggested of containing a homozygous losses/deletion as $\log_2$ ratio less than −1.0. We defined region of gain or loss as (1) continuously ordered 3 clones showing gain or loss or as (2) single clones showing recurrent high copy number gain ($\log_2$ ratio > +1.0) or homozygous loss ($\log_2$ ratio < −1.0).[11,12]

Regions of high-level gain and regions of homozygous loss/deletion were also easily detected, as were regions showing low-level gain and those of heterozygous loss/deletion.

Statistical analysis

Statistical analysis of overall survival of distinct subgroups of DLBCL was conducted by log-rank test. *P* less than .05 was taken to show a significant difference.

Statistical analysis for array CGH. To analyze genomic regions for statistically significant differences between the 2 patient groups (eg, ABC and GCB), a data set was constructed by defining genomic alterations as copy number gains for $\log_2$ ratio thresholds of +0.2 or greater, and as copy number losses for thresholds of −0.2 or less. Clones showing a gain ($\log_2$ ratio ≥ +0.2) were inputted as " 1 " versus no-gain clones ($\log_2$ ratio < +0.2) as " 0 " on an Excel (Microsoft, Redman, WA) template for each case. Similarly, loss clones ($\log_2$ ratio ≤ −0.2) were inputted as "1" versus no-loss clones ($\log_2$ ratio > −0.2) as " 0 " on another Excel template for each case. Data analyses were then carried out for the following purposes: (1) comparison between the 2 groups (eg, ABC and GCB) of frequencies of gain or loss for each single clone, and (2) comparison of overall survival between cases showing gain or loss of a single clone and cases without either gain or loss. Fisher exact test for probability was used for the former comparison, and a log-rank test for comparing survival curves for the 2 groups was used for the latter.

Statistical analysis for gene-expression profiling. The Mann-Whitney *U* test was performed for detecting significant differences in expression levels of $p16^{INK4a}$ between the ABC and GCB groups. All the statistical analyses were conducted with the STATA version 8 statistical package (StataCorp, College Station, TX).

Results

Gene-expression profiling of CD5+, CD5−CD10+, and CD5−CD10−DLBCL: relationship with ABC and GCB DLBCLs

The variety of DLBCLs can be characterized and classified by gene-expression profiling and cell-surface phenotyping. Clinically, ABC DLBCL behaves more aggressively than GCB DLBCL. The survival of CD5+ DLBCL cases is shorter, and CD10+ DLBCL is relatively indolent (Figure 1).

To determine whether DLBCL with CD5 and/or CD10 markers are related to the ABC and GCB subgroups, we subjected a total of 46 DLBCL cases (22 cases of CD5+, 7 cases of CD5−CD10+, and 17 cases of CD5−CD10−) to gene-expression profiling. The results showed that the 46 cases could be clearly assigned to either the ABC or GCB groups (Figure 2) and, of special importance, that the CD5+ and CD5−CD10+ phenotypes were closely related to the ABC and GCB subgroups, respectively (Table 2). Of the 22 CD5+ DLBCL cases, 19 showed the ABC signature, whereas only 3 were characterized by the GCB signature (2 cases of CD5+CD10+ and 1 case of CD5+CD10−) ($P = .001$). In sharp contrast, all 7 cases of CD5−CD10+ DLBCL showed the GCB signature ($P = .003$). CD5−CD10− DLBCL cases showed mixed results, expressing either the ABC (9 cases) or GCB (8 cases) signature ($P = .533$), indicating that it is a heterogeneous entity.

Genomic imbalance of ABC and GCB DLBCLs

Because it was previously demonstrated that ABC and GCB DLBCLs are molecularly distinct subgroups,[6-8] we initially compared the genomic profiles of these subgroups. Two typical individual genomic profiles of 2 CD5−CD10− cases, 1 with an ABC signature and the other with a GCB signature, are shown in Figure 3.

Frequent genomic imbalances (copy number changes) of the ABC group (≥ 6 cases) were gain of chromosome 3, 8q21-q26, 11q21-q25, 16p11-p13, 16q22-q24, 18, 19q13 and X, and loss of 2p11 (Ig*k* locus), 6q12-q27, 8p22-p23, 9p21, and 17p. Frequent genomic imbalances of the GCB group (≥ 4 cases) were gain of 1q22-q32, 2p14-p24, 5p12-p15, 5q15-q31, 6p12-p25, 7, 8q22-q26, 9q33-q34, 11q, 12, 13q31-q33, 16p11-p13, 18q21-q23, 19p, 19q13, 21q, and X and loss of 1p36, 2p11, 3p14, 4p12-p13, 4q33-q34, 6q14-q16, 8p22-p23, 9p21, 13q12-q22, 17p12, and 18q22-q23. Here, frequent genomic gains and losses were defined as greater than 20% for either group.

The ABC group was genomically characterized by more frequent gains of 3p23-q28, 18q11.2-q23, and 19q13.41-q13.43 and loss of 6q22.31-q24.1 and 9p21.3. The GCB group was genomically characterized by more frequent gains of 1q21.1-q23.3, 1q31.1-q42.13, 2p15-p16.1, 7q22.1-q36.2, and 12q13.1-q14 (Fisher

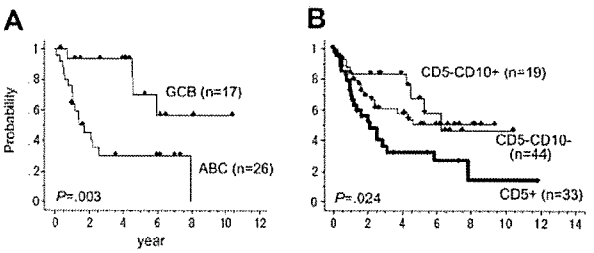

Figure 1. Kaplan-Meier analyses of different subgroups. (A) Kaplan-Meier analysis of ABC (26 cases) and GCB (17 cases) DLBCLs. (B) Kaplan-Meier analysis of CD5+ (33 cases), CD5−CD10+ (19 cases), and CD5−CD10− (44 cases) DLBCLs. The *P* values were obtained by a log-rank test. The overall survival of 96 cases could be analyzed. This showed that the overall survival for the CD5+ group was worse than that of the CD5−CD10+ and CD5−CD10− groups (log-rank test, $P = .023$). There was no significant difference in the overall survival between the CD5−CD10− and the CD5−CD10+ groups (log-rank test, $P = .504$). Expression profiling was performed for 46 cases, 43 of which could be analyzed for overall survival. This indicated that the overall survival for the ABC group was worse than that of the GCB group ($P = .003$).

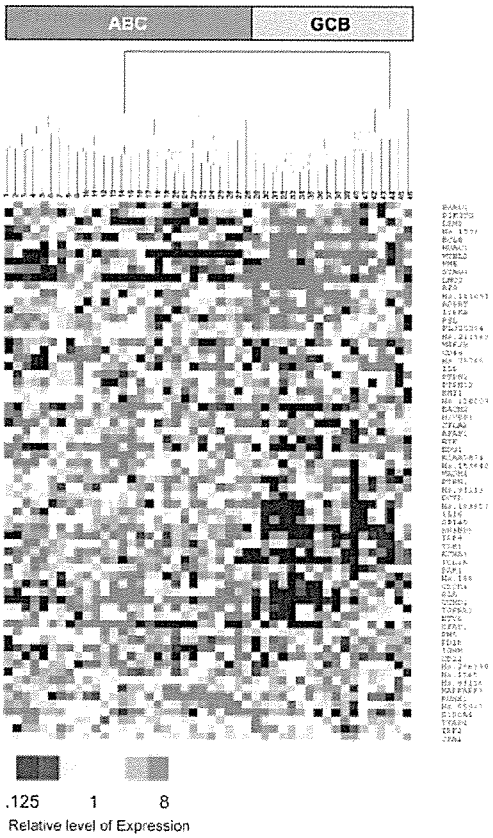

Figure 2. Hierarchical clustering of 46 DLBCL cases. A total of 46 cases (22 of CD5$^+$, 7 of CD5$^-$CD10$^+$, and 17 of CD5$^-$CD10$^-$) were clustered with the aid of Tree View software, based on the expression of 67 of 100 genes as described by Rosenwald et al.[8] The degree of relative expression of the gene for each sample is indicated at the bottom. The samples were divided into 2 subgroups, ABC (left) and GCB (right).

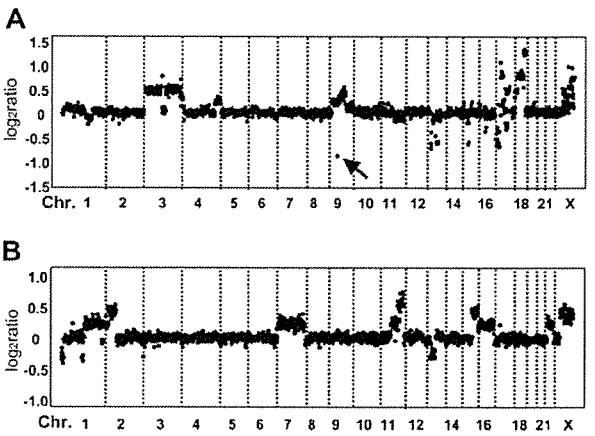

Figure 3. Typical individual genome profiles of DLBCL cases. The individual genomic profile of 2 CD5$^-$CD10$^-$ cases, 1 with an ABC signature (A) and the other with a GCB signature (B). Chr. indicates chromosome number. (A) Genomic gains are the following: 3p26.3-q12.3, 3q13.33-q29, 4q32.1-q35.1, 9p24.3-q22.33, 17p11.2-q21.1, 17q21.32, 17q23.2-q24.2, 18q, and Xp22.11-q28; genomic losses are the following: 9p21.3 (arrow), 13q14.3-q21.2, 15q21.3, 17p11.2-p13.3, and 17q21.33-q22. Note that loss of 9p21 occurred only at BAC, RP11-149I2 (arrow), which contains *p16^{INK4a}*. (B) Genomic gains are the following: 1q21.3-q44, 2p13.2-p25.1, 7, 11q13.5-q25, 15q24.3-q26.3, 16, 21q, and X; genomic losses are the following: 1p36.22-p36.33, 1p13.1-p31.2, and 13q13.1-q14.3.

exact test, $P < .05$). Ideogram of the genomic imbalance of ABC and GCB DLBCLs are presented in Figure 4A-B, and the genome-wide frequency representing the genomic imbalance of ABC and GCB DLBCL are presented in Figure 5A.

We found that the genomic imbalance patterns of ABC and GCB DLBCLs are distinctly different. For instance, gain of chromosome 3q23-q28 was observed in 25% to 36% of the ABC group but not in the GCB group (0%), whereas gain of 7q22-q36 was observed in 50% to 61% of the GCB group and far less (< 5%) in the ABC group.

It should be noted that the expression of CD5 had no effect on the genomic imbalance observed in the ABC and GCB groups. The genomic imbalance detected here in the ABC group reflects the dominance of CD5-classified cases: 67% (19 of 28 cases) of the ABC group was of the CD5$^+$ type, but the frequency and region of the genomic imbalance of CD5$^+$ and CD5$^-$ within the ABC group were similar. There were no significant differences in either region or frequency of the genomic imbalance between CD5$^+$ and CD5$^-$ within the ABC group (data not shown). A typical example was loss of 9p21. This loss was specific to the ABC group where, within the ABC group, 13 (68%) of the 19 CD5$^+$ DLBCL cases and 6 (66%) of the 9 CD5$^-$ DLBCL cases showed this loss ($P = 0.999$).

Table 2. Relationship among DLBCL subgroups differentiated by gene-expression profiling

DLBCL subtype	ABC	GCB	*P*
CD5$^+$*	19	3	.001
CD5$^-$CD10$^+$	0	7	.003
CD5$^-$CD10$^-$	9	8	.533

P values were obtained by Fisher exact test.
*CD5$^+$ DLBCL includes 3 of CD10$^+$ cases.

Genomic imbalance of CD5$^+$, CD5$^-$CD10$^+$, and CD5$^-$CD10$^-$ DLBCLs

We examined the frequency of gain and loss regions for the CD5$^+$ (36 cases), CD5$^-$CD10$^+$ (19 cases), and CD5$^-$CD10$^-$ (44 cases) groups. Frequent genomic imbalances (≥ 8 cases) in the CD5$^+$ group were gain of chromosome 3, 6p22-p25, 7p22-q31, 8q24, 11q22-q25, 12, 16p13-q21, 18, 19, and X and loss of 1p36, 2p11, 6q14-q27, 8p23, 9p21, 15q13-q14, and 17p11-p13. Although gain of 1q21-q32, 7p22-q36, and 12 were characteristic of the GCB group, these gains were also found in 20% or less of the CD5$^+$ group.

Frequent genomic imbalances (≥ 4 cases) in the CD5$^-$CD10$^+$ group were gain of 1q, 2p13-p25, 6p21-p25, 7, 8q22-q24, 9q33-q34, 12, 13q31-q33, 15q, 16p13, 19q13.3-q13.4, and X and loss of 1p36, 1p22, 2p11, 3p14, 4p, 6q13-q27, 9p21, and 13q14-q21.

Comparison of the CD5$^+$ and CD5$^-$CD10$^+$ subgroups showed that CD5$^+$ DLBCL had more frequent gains at chromosome 3 and loss of 9p21 compared with CD5$^-$CD10$^+$ DLBCL, whereas CD5$^-$CD10$^+$ DLBCL showed more frequent gains of 7q22-q36, 12q13-q14, and 17p13 compared with CD5$^+$ DLBCL (Table 3). The genome-wide frequency of the genomic imbalance of CD5$^+$ and CD5$^-$CD10$^+$ DLBCLs are shown in Figure 5B. Of special importance is that these characteristic genomic profiles of CD5$^+$ and CD5$^-$CD10$^+$ DLBCLs are quite similar to those of ABC and GCB DLBCLs, respectively (Figure 5A-B). There were no significant differences in either region or frequency of genomic

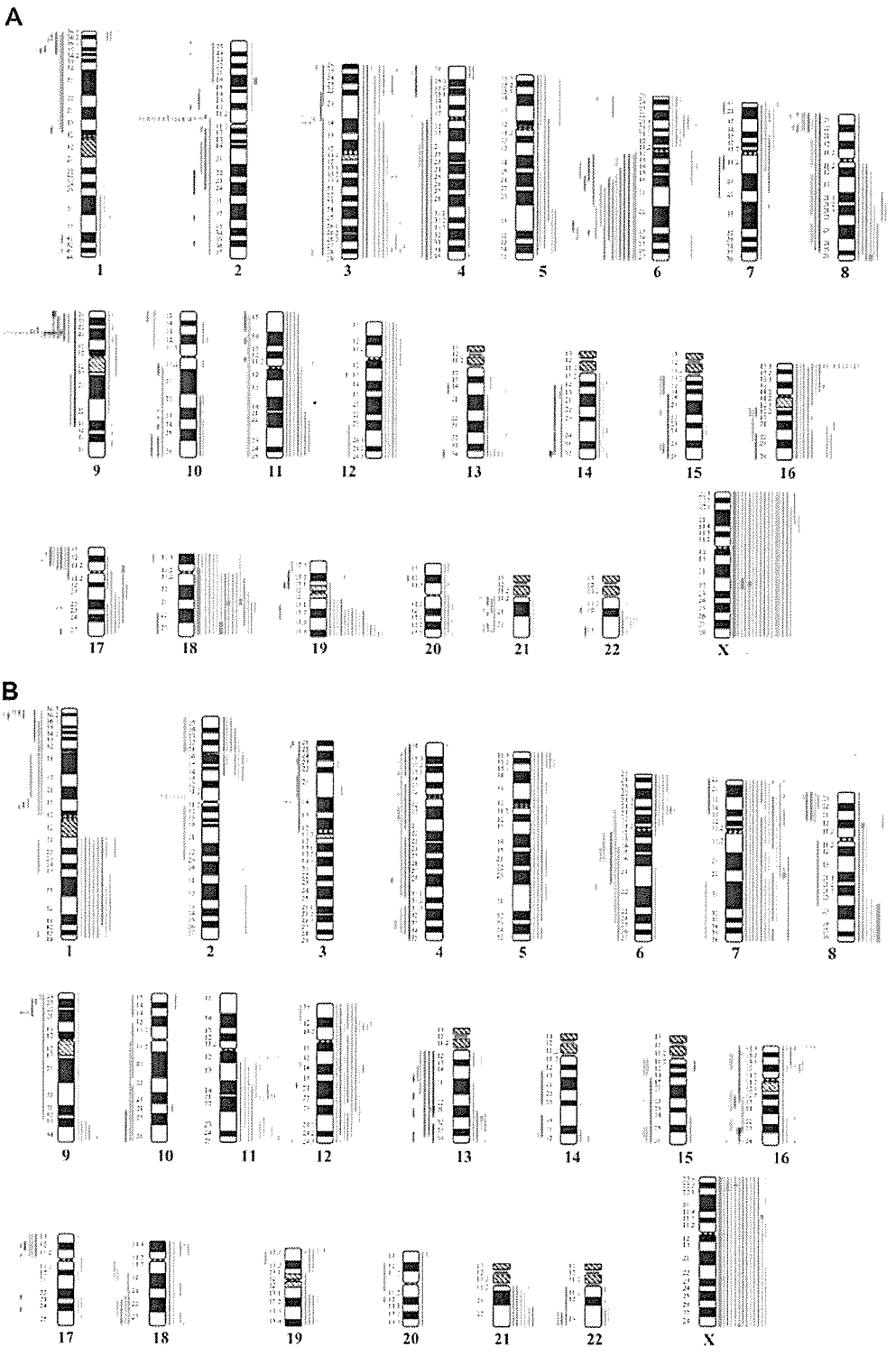

Figure 4. Ideogram of the genomic imbalance of ABC and GCB DLBCLs. Summary of the chromosomal imbalance of 28 patients in the ABC group (A) and 18 patients in the GCB group (B). Lines on the left (red) of the ideogram indicate losses, and those on the right (green) indicate gains. Red squares represent homozygous losses ($\log_2$ ratio < -1.0) on the left, and green squares high-level gains ($\log_2$ ratio $> +1.0$) on the right.

imbalance between either the $CD5^+$ and ABC groups or the $CD5^-CD10^+$ and GCB groups (Table 3).

Frequent genomic imbalance of the $CD5^-CD10^-$ group (≥ 9 cases) was gain of 1q21-q42, 3q21-q29, 5p13-p15, 6p21-p25, 7, 11q22, 12q13-q14, 18, 19q13.1-q13.4, and X and loss of 2p11, 3p14.2, 6q12-q27, 9p21.3, 15q14-q15, and 17p11-p13. The genomic imbalance of $CD5^-CD10^-$ DLBCL reflected a mixed type because all of these gains and losses could be observed in both the $CD5^+$ and $CD5^-CD10^+$ groups. Furthermore, the frequency and region of the genomic imbalance of $CD5^-CD10^-$ DLBCL was very similar to that of ABC plus GCB, as shown in Figure 5. There were no significant differences in either region or frequency of the genomic imbalance between the $CD5^-CD10^+$ and ABC plus GCB groups (data not shown). These findings correlate well with the results of gene-expression profiling that showed $CD5^-CD10^-$ DLBCL was evenly distributed in the ABC and GCB groups.

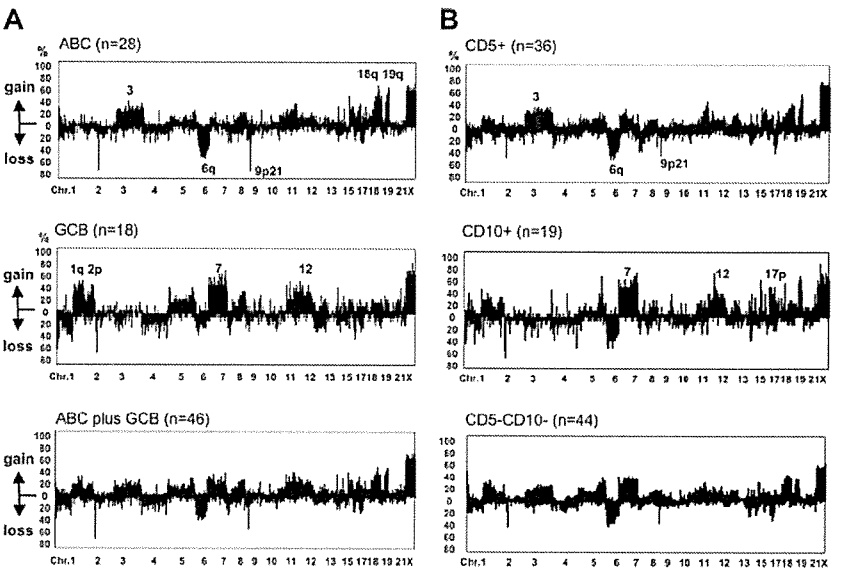

Figure 5. Genome-wide frequency of the genomic imbalance in distinct DLBCL subtypes. Horizontal lines indicate 2213 BAC/PAC clones in order from chromosomes 1 to 22 and X. Within each chromosome, clones are shown in order from the p telomere to the q telomere according to information from the Ensemble Genome Data Resources of Sanger Center Institute, November 2004 version. Vertical lines indicate frequency (%) of gains and losses. (A) ABC group (28 cases), GCB group (18 cases), and ABC plus GCB (46 cases). (B) $CD5^+$ group (36 cases), $CD5^-CD10^+$ group (19 cases), and $CD5^-CD10^-$ group (44 cases). The genomic imbalance characteristic of the $CD5^+$ and $CD5^-CD10^+$ groups was similar to those of the ABC and GCB groups, respectively. Frequency and region of the genomic imbalance of $CD5^-CD10^-$ DLBCL showed patterns similar to that of ABC plus GCB.

Identification of loss of 9p21 ($p16^{INK4a}$ locus) as a strong prognostic marker

Finally, we tried to identify prognostic variables detected by the array CGH and found that loss of 9p21 had a deleterious effect on patient survival: 37 cases with loss of 9p21 showed significantly poorer survival than the 59 cases without this loss (log-rank test, $P = 0.001$) (Figure 6A).

Loss of 9p21 was significantly more frequently detected in the ABC group (19 cases) than in the GCB group (5 cases) (Fisher exact test, $P = .014$). The survival of ABC cases with loss of 9p21 was significantly inferior to that of the ABC cases without such a loss (log-rank test, $P = .013$), whereas loss at the corresponding region in the GCB group did not affect survival. Similarly, the survival of $CD5^+$ cases with loss of 9p21 was significantly poorer than cases without this loss (log-rank test, $P = .004$). Thus we were able to show that loss of 9p21 ($p16^{INK4a}$ locus) marks the most aggressive form of DLBCL. Among the $CD5^-CD10^-$ DLBCL cases, loss of 9p21 tended to have a negative effect on survival, although this did not reach statistical significance (log-rank test, $P = .068$).

As shown in Figure 6B, the minimum common region of 9p loss was located within 2.2 Mb at 9p21.3. Evidence suggesting homozygous losses of 9p21 was found in 6 cases (defined as $\log_2$ ratio < -1.0; 3 cases each of $CD5^+$ and $CD5^-CD10^-$), whereas all GCB or $CD5^-CD10^+$ cases failed to show any signs, suggesting homozygous loss at 9p21.3. Thirteen of the 37 cases with loss of 9p21 showed loss at a restricted position of the genome encompassing a single BAC, RP11-149I2, which contains the $p16^{INK4a}$ tumor suppressor. The expression level of $p16^{INK4a}$ for the ABC group was significantly lower than that of the GCB group (Figure 6C) (Mann-Whitney U test, $P = .001$). These results agree well with the finding of a higher frequency of 9p21.3 loss in ABC DLBCL cases.

Discussion

Several researchers have reported genomic alterations in DLBCL detected by means of conventional CGH or array CGH.[14-18] However, only a few comparative genome analyses of DLBCL subtypes have been conducted.[12,19] In the study presented here, our array CGH enabled us to detect distinct differences in the genomic imbalance patterns of the ABC and GCB subgroups. ABC DLBCL is genomically characterized by gain of 3q, 18q, and 19q and loss of

Table 3. Characteristic genomic imbalances and comparison of frequencies among DLBCL subgroups

Chromosome	Gain/loss	Minimum common region	ABC, no. cases (%)	GCB, no. cases (%)	$CD5^+$, no. cases (%)	$CD5^-CD10^+$, no. cases (%)	Fisher P: ABC vs GCB	Fisher P: $CD5^+$ vs $CD10^+$
1	Gain	1q21.1-q23.3	0 (0)	8 (44)	6-7 (17-19)	5-7 (26-37)	< .01	NS
1	Gain	1q31.1-q42.13	2 (0-7)	8-9 (44-50)	5-6 (14-17)	6-7 (32-37)	< .01	NS
2	Gain	2p15-p16.1	2 (7)	6 (33)	4-8 (11-22)	5-8 (26-42)	.04	NS
3	Gain	3q23-q28	7-10 (25-36)	0 (0)	11 (31)	0-1 (0-5)	.03	.01-.04
6	Loss	6q22.31-q24.1	11-13 (39-46)	2 (11)	16 (44)	12 (63)	.02-.04	NS
7	Gain	7q22.1-q36.2	1 (4)	9-11 (50-61)	4-6 (11-17)	9-11 (47-58)	< .01	< .01
9	Loss	9p21.3	19 (68)	5 (28)	18 (50)	4 (21)	.01	.04
12	Gain	12q13.13-q14.1	4 (14)	8 (44)	5-6 (14-17)	9-13 (47-68)	.04	< .02
17	Gain	17p13.1	5 (18)	3 (17)	2 (6)	7 (37)	NS	< .01
18	Gain	18q11.2-q23	13-15 (46-54)	3-4 (17-22)	14-15 (38-42)	5 (26)	.03	NS
19	Gain	19q13.32-q13.33	13 (46)	3 (17)	12 (33)	12 (63)	NS	NS
19	Gain	19q13.41-q13.42	15 (54)	3 (17)	17 (47)	12 (63)	.01	NS

For ABC, n = 28; for GCB, n = 18; for $CD5^+$, n = 36; for $CD5^-CD10^+$, n = 19.
NS indicates not significant; no. cases, the number of cases showing genomic gains and losses within each minimum common region.

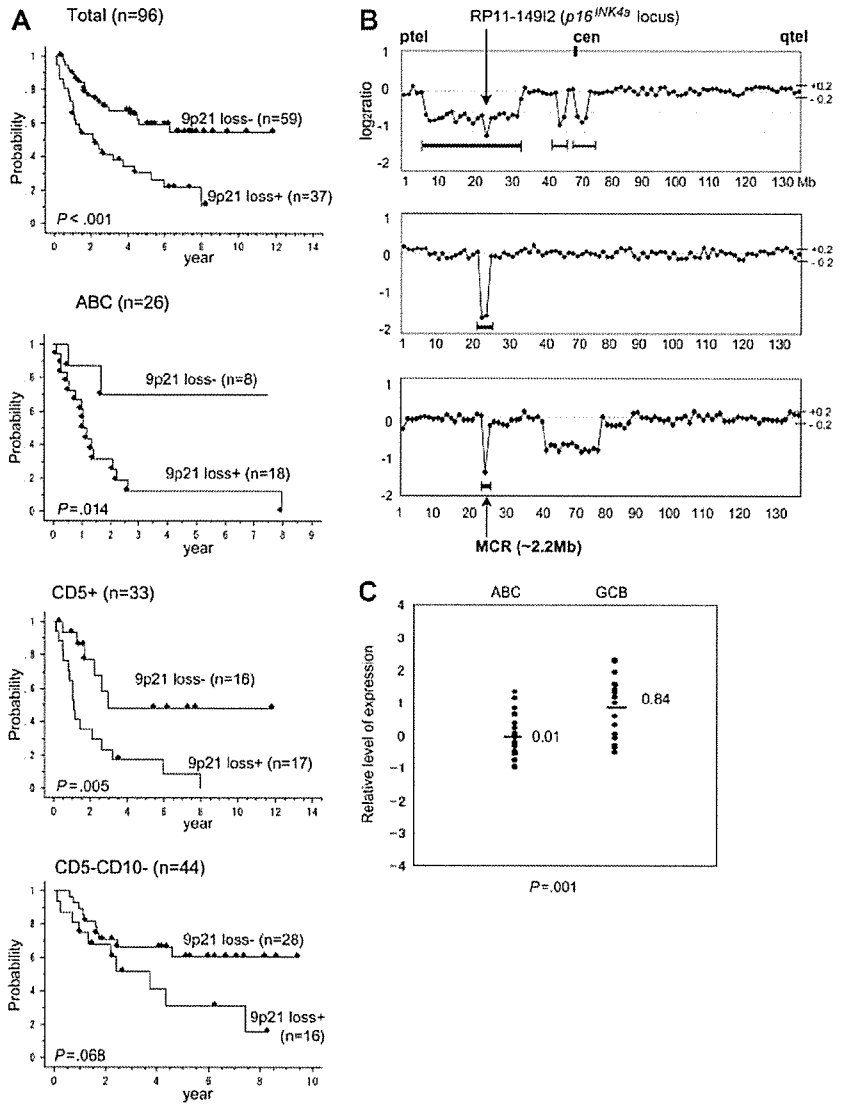

Figure 6. Genomic loss of 9p21.3, overall survival, and comparison of *p16*^{INK4a} gene expression in the ABC and GCB groups. (A) Kaplan-Meier analyses of survival of total cases, ABC cases, CD5$^+$ cases, and CD5$^-$CD10$^-$ cases either with or without 9p21.3 (*p16*^{INK4a} locus) loss. (B) Representative individual genome profile of 9p21 in 3 cases. Dots represent the $\log_2$ ratio of BAC/PAC clones, which are shown in order from the p telomere to the q telomere. Bold lines under each profile indicate regions of loss. MCR indicates minimum common region of 9p loss. Vertical lines indicate $\log_2$ ratio; horizontal lines, megabases. Threshold of $\log_2$ ratio is $-0.2 < \log_2 \text{ ratio} < +0.2$. (C) Comparison of *p16*^{INK4a} expression in the ABC and GCB groups. Statistical significance of the difference was calculated using the Mann-Whitney *U* test. Horizontal bars indicate the mean value of relative level of expression.

6q and 9p21, whereas GCB DLBCL is genomically characterized by gain of 1q, 2p, 7q, and 12q. These results thus provide evidence that the ABC and GCB groups are genetically distinct to each other, suggesting that ABC and GCB DLBCL develop tumors via distinct genomic pathways.

Four groups have published reports on the genomic imbalance of DLBCL transformed from follicular lymphoma (FL).[18,20-22] According to their reports, DLBCL transformed from FL is characterized by a genomic imbalance consisting of gain of 2p, 7p, 12p, and 12q and loss of 4q and 13q. Because the characteristic genomic imbalance of DLBCL transformed from FL is similar to that of the GCB group, DLBCL transformed from FL and GCB DLBCL may share certain steps in their genomic aberration program through the development of lymphomagenesis.

We previously reported that CD5$^+$ and CD10$^+$ DLBCL constitute clinically relevant subtypes. In the study presented here, we report for the first time that CD5$^+$ DLBCL is characterized by ABC expression and unique genomic patterns. Recently, Katzenberger et al[23] conducted a cytogenetic and loss of heterozygosity study of de novo CD5$^+$ DLBCL and speculated that CD5$^+$ DLBCL was likely to originate from the same progenitor cells as B-chronic lymphocytic leukemia (CLL) because the former showed frequent deletions of the *D13S25* locus as well as of the *p16*^{INK4a} tumor suppressor.[23] However, CD5$^+$ DLBCL appears to be different both in terms of its origin and pathway from CLL and mantle cell lymphoma (MCL), which also express CD5. CLL and MCL are both characterized by loss of 6q, 9p21, 11q22-q23, and 13q14-q21 (seen in 30%-50% of cases),[24-27] whereas less than 10% of CD5$^+$ DLBCL cases examined by us showed loss of 11q22-q23, and 13q14-q21. Loss of only *p16*^{INK4a} appears to be a common characteristic.

We were also able to demonstrate that CD10$^+$ DLBCL is characterized by GCB expression and unique genomic patterns. We previously reported that CD10$^+$ DLBCL might originate from germinal center progenitor cells because cells with a normal follicular center possess CD5$^-$ and CD10$^+$ immunophenotypes and rarely express BCL2. Huang et al[28] used gene-expression profiling to demonstrate that CD10$^+$ DLBCL is characterized by a GCB signature, as is also evident from our results.[28,29]

We noted that CD5$^-$CD10$^-$ DLBCL exhibited a mixed genomic imbalance pattern with respect to 2 subtypes (CD5$^+$ and CD5$^-$CD10$^+$). This correlates well with the results of gene-expression profiling, which showed that CD5$^-$CD10$^-$ DLBCL was

evenly distributed within the ABC or GCB groups, suggesting that $CD5^-CD10^-$ DLBCL is a genetically heterogeneous entity.

Loss of 9p21 ($p16^{INK4a}$) may mark the most aggressive cases. Of special interest in our series was that ABC and $CD5^+$ DLBCL cases with loss of 9p21 showed poorer outcomes than cases without this loss. Loss of 9p21 may therefore represent a unique feature, reflecting the most aggressive form of DLBCL. Deletion of 9p21.3 ($p16^{INK4a}$ locus) is frequently found in aggressive lymphoma and acute lymphoblastic leukemia and less often in low-grade lymphoma.[30-35] $CD5^+$ DLBCL is also closely associated with many aggressive clinical features or parameters, and loss of 9p21 in conjunction with inactivation of $p16^{INK4a}$ may well be a feature of $CD5^+$ DLBCL. Indeed, frequent deletion of 9p21 in $CD5^+$ DLBCL has been reported by us and another group.[12,23]

To summarize, we were able to demonstrate that ABC and GCB DLBCLs are distinct in terms of gene expression and genomic imbalance. Most of the $CD5^+$ and $CD5^-CD10^+$ DLBCLs are included in the ABC and GCB groups, respectively. Furthermore, when searching for genomic imbalances that affect patient prognosis, we found that loss of 9p21 ($p16^{INK4a}$ locus) marks the most aggressive form of DLBCL. As demonstrated with DLBCL, the combined use of gene-expression profiling and array CGH may facilitate better understanding of heterogeneous tumors in general.

Acknowledgments

We thank Mss H. Suzuki and Y. Kasugai for their outstanding technical assistance. We also thank Dr Ryuzo Ohno, president of the Aichi Cancer Center, for his support.

References

1. Harris NL, Jaffe ES, Stein H, et al. A revised European-American classification of lymphoid neoplasms: a proposal from the International Lymphoma Study Group. Blood. 1994;84:1361-1392.
2. Offit K, Le Coco F, Louie DC, et al. Rearrangement of BCL6 gene as a prognostic marker in diffuse large cell lymphoma. N Engl J Med.1994; 331:74-80.
3. Kramer MHH, Hermans J, Wijburg E, et al. Clinical relevance of BCL2, BCL6, and MYC rearrangements in diffuse large B-cell lymphoma. Blood. 1998;92:3152-3162.
4. Gatter KC, Warnke RA. Diffuse large B-cell lymphoma. In: Jaffe ES, Harris NL, Stein H, Vardiman JW, eds. World Health Classification of Tumors. Pathology and Genetics of Tumors of Haematopoietic and Lymphoid Tissues. Lyon, France: IARC Press; 2001:171-174.
5. Fisher RI, Gaynor ER, Dahlberg S, et al. Comparison of a standard regimen (CHOP) with three intensive chemotherapy regimens for advanced non-Hodgkin's lymphoma. N Engl J Med. 1993; 328:1002-1006.
6. Alizadeh AA, Eisen MB, Davis RE, et al. Distinct types of diffuse large B-cell lymphoma identified by gene expression profiling. Nature. 2000;403: 503-511.
7. Wright G, Tan B, Rosenwald A, et al. A gene expression-based method to diagnose clinically distinct subgroups of diffuse large B cell lymphoma. Proc Natl Acad Sci U S A. 2003;100:9991-9996.
8. Rosenwald A, Wright G, Chan WC, et al. The use of molecular profiling to predict survival after chemotherapy for diffuse large-B-cell lymphoma. N Engl J Med. 2002;346:1937-1947.
9. Harada S, Suzuki R, Uehira K, et al. Molecular and immunological dissection of diffuse large B cell lymphoma: $CD5^+$ and CD5 with $CD10^+$ groups may constitute clinically relevant subtypes. Leukemia. 1999;13:1441-1447.
10. Yamaguchi M, Seto M, Okamoto M, et al. De novo $CD5^+$ diffuse large B-cell lymphoma: a clinicopathologic study of 109 patients. Blood. 2002; 99:815-821.
11. Ota A, Tagawa H, Karnan S, et al. Identification and characterization of a novel gene, *C13orf25*, as a target for 13q31-q32 amplification in malignant lymphoma. Cancer Res. 2004;64:3087-3095.
12. Tagawa H, Tsuzuki S, Suzuki R, et al. Genome-wide array-based comparative genomic hybridization of diffuse large B-cell lymphoma: comparison between CD5-positive and CD5-negative cases. Cancer Res. 2004;64:5948-5955.
13. Eisen MB, Spellman PT, Brown PO, et al. Cluster analysis and display of genome-wide expression patterns. Proc Natl Acad Sci U S A. 1998;95: 14863-14868.
14. Monni O, Joensuu H, Franssila K, Knuutila S. DNA copy number changes in diffuse large B-cell lymphoma-comparative genomic hybridization study. Blood. 1996;87:5269-5278.
15. Rao PH, Houldsworth J, Dyomina K, et al. Chromosomal and gene amplification in diffuse large B-cell lymphoma. Blood. 1998;92:234-240.
16. Berglund M, Enblad G, Flordal E, et al. Chromosomal imbalances in diffuse large B-cell lymphoma detected by comparative genomic hybridization. Mod Pathol. 2002;15:807-816.
17. Bea S, Colomo L, Lopez-Guillermo A, et al. Clinicopathologic significance and prognostic value of chromosomal imbalances in diffuse large B-cell lymphomas. J Clin Oncol. 2004;22:3498-3560.
18. Martinez-Climent JA, Alizadeh AA, Segraves R, et al. Transformation of follicular lymphoma to diffuse large cell lymphoma is associated with a heterogeneous set of DNA copy number and gene expression alterations. Blood. 2003;101: 3109-3117.
19. Zang X, Karnan S, Tagawa H, et al. Comparison of genetic aberrations in $CD10^+$ diffuse large B-cell lymphoma and follicular lymphoma by comparative genomic hybridization and tissue-fluorescence in situ hybridization. Cancer Sci. 2004; 95:809-814.
20. Goff LK, Neat MJ, Crawley CR, et al. The use of real-time quantitative polymerase chain reaction and comparative genomic hybridization to identify amplification of the REL gene in follicular lymphoma. Br J Haematol. 2000;111:618-625.
21. Nagy M, Balazs M, Adam Z, et al. Genetic instability is associated with follicle center lymphoma. Leukemia. 2000;14:2142-2148.
22. Hough RE, Goepel JR, Alcock HE, Hancock BW, Lorigan PC, Hammond DW. Copy number gain at 12q12–14 may be important in the transformation from follicular lymphoma to diffuse large B cell lymphoma. Br J Cancer. 2001;84:499-503.
23. Katzenberger T, Lohr A, Schwarz S, et al. Genetic analysis of de novo $CD5^+$ diffuse large B-cell lymphomas suggests an origin from a somatically mutated $CD5^+$ progenitor B cell. Blood. 2003; 101:699-702.
24. Bentz M, Plesch A, Bullinger L, et al. t(11;14)-positive mantle cell lymphomas exhibit complex karyotypes and share similarities with B-cell chronic lymphocytic leukemia. Genes Chromosomes Cancer. 2000;27:285-294.
25. Schwaenen C, Nessling M, Wessendorf S, et al. Automated array-based genomic profiling in chronic lymphocytic leukemia: development of a clinical tool and discovery of recurrent genomic alterations. Proc Natl Acad Sci U S A. 2004;101: 1039-1044.
26. Kohlhammer H, Schwaenen C, Wessendorf S, et al. Genomic DNA-chip hybridization in t(11;14)-positive mantle cell lymphomas shows a high frequency of aberrations and allows a refined characterization of consensus regions. Blood. 2004; 104:795-801.
27. Tagawa H, Karnan S, Suzuki R, et al. Genome-wide array-based CGH for mantle cell lymphoma: identification of homozygous deletions of the pro-apoptotic gene *BIM*. Oncogene. 2005;24:1348-1358.
28. Huang JZ, Sanger WG, Greiner TC, et al. The t(14;18) defines a unique subset of diffuse large B-cell lymphoma with a germinal center B-cell gene expression profile. Blood. 2002;99:2285-2290.
29. Iqbal J, Sanger WG, Horsman DE, et al. BCL2 translocation defines a unique rumor subset within the germinal center B-cell-like diffuse large B-cell lymphoma. Am J Pathol. 2004;165:159-166.
30. Serrano M, Hannon GJ, Beach D. A new regulatory motif in cell-cycle control causing specific inhibition of cyclin D/CDK4. Nature. 1993;366: 704-707.
31. Nobori T, Miura K, Wu DJ, et al. Deletions of the cyclin-dependent kinase-4 inhibitor gene in multiple human cancers. Nature. 1994;368:753-756.
32. Koduru PR, Zariwala M, Soni M, et al. Deletion of cyclin-dependent kinase 4 inhibitor genes p15 and p16 in non-Hodgkin's lymphoma. Blood. 1995;86:2900-2905.
33. Stranks G, Height SE, Mitchell P, et al. Deletions and rearrangement of CDKN2 in lymphoid malignancy. Blood. 1995;85:893-901.
34. Ogawa S, Hangaishi A, Miyawaki S, et al. Loss of the cyclin-dependent kinase 4-inhibitor (p16; MTS1) gene is frequent in and highly specific to lymphoid tumors in primary human hematopoietic malignancies. Blood. 1995;86:1548-1556.
35. Pinyol M, Cobo F, Bea S, et al. p16 (INK4a) gene inactivation by deletions, mutations, and hypermethylation is associated with transformed and aggressive variants of non-Hodgkin's lymphomas. Blood. 1998;91:2977-2984.

Oncogene (2005) 24, 1348–1358

www.nature.com/onc

Genome-wide array-based CGH for mantle cell lymphoma: identification of homozygous deletions of the proapoptotic gene *BIM*

Hiroyuki Tagawa[1], Sivasundaram Karnan[1], Ritsuro Suzuki[1], Keitaro Matsuo[2], Xiaohua Zhang[1,5], Akinobu Ota[1,6], Yasuo Morishima[3], Shigeo Nakamura[4] and Masao Seto*[,1]

[1]*Division of Molecular Medicine, Aichi Cancer Center Research Institute, 1-1-1 Kanokoden, Chikusa-ku, Aichi, Nagoya 464-8681, Japan;* [2]*Division of Epidemiology, Aichi Cancer Center Research Institute, 1-1-1 Kanokoden, Chikusa-ku, Aichi, Nagoya 464-8681, Japan;* [3]*Department of Hematology and Chemotherapy, Aichi Cancer Center Hospital, Aichi 464-8681, Japan;* [4]*Department of Pathology and Molecular Diagnostics, Aichi Cancer Center Hospital, Aichi 464-8681, Japan;* [5]*Department of Pathology, Yan'an University School of Medicine, Yan'an 716000, PR China;* [6]*Immuno-Biological Laboratories Co., Ltd, Gunma 375-0005, Japan*

Mantle cell lymphoma (MCL) is characterized by 11q13 chromosomal translocation and *CCND1* overexpression, but additional genomic changes are also important for lymphomagenesis. To identify the genomic aberrations of MCL at higher resolutions, we analysed 29 patient samples and seven cell lines using array-based comparative genomic hybridization (array CGH) consisting of 2348 artificial chromosome clones, which cover the whole genome at a 1.3 mega base resolution. The incidence of identified genomic aberrations was generally higher than that determined with chromosomal CGH. The most frequent imbalances detected by array CGH were gains of chromosomes 3q26 (48%), 7p21 (34%), 6p25 (24%), 8q24 (24%), 10p12 (21%) and 17q23 (17%), and losses of chromosomes 2p11 (83%), 11q22 (59%), 13q21 (55%), 1p21–p22 (52%), 13q34 (52%), 9q22 (45%), 17p13 (45%), 9p21 (41%), 9p24 (41%), 6q23–q24 (38%), 1p36 (31%), 8p23 (34%), 10p14 (31%), 19p13 (28%), 5q21 (21%), 22q12 (21%), 1q42 (17%) and 2q13 (17%). Our analyses also detected several novel recurrent regions of loss located at 1p36, 1q42.2–q43, 2p11.2, 2q13, 17p13.3 and 19p13.2–p13.3, as well as recurrent regions of homozygous loss such as 2p11 (*Igκ*), 2q13 and 9p21.3–p24.1 (*INK4a/ARF*). Of the latter, we investigated the 2q13 loss, which led to identification of homozygous deletions of the proapoptotic gene *BIM*. The high-resolution array CGH technology allowed for the precise identification of genomic aberrations and identification of *BIM* as a novel candidate tumor suppressor gene in MCL.
Oncogene (2005) **24,** 1348–1358. doi:10.1038/sj.onc.1208300
Published online 20 December 2004

Keywords: mantle cell lymphoma; array CGH; *BIM*; 2q13; chromosome alteration

*Correspondence: M Seto; E-mail: mseto@aichi-cc.jp
Received 14 July 2004; revised 6 September 2004; accepted 19 October 2004; published online 20 December 2004

Introduction

Mantle cell lymphoma (MCL) is characterized by t(11;14)(q13;q32), which results in overexpression of *CCND1*, and is presumed to derive from naive pregerminal center CD5$^+$ B cells (Seto *et al.*, 1992; Jaffe *et al.*, 2001). The identification of this translocation in virtually all cases of MCL with *CCND1* overexpression indicates that this genomic alteration is an important mechanism for its pathogenesis (Jaffe *et al.*, 2001). Despite the presence of this common molecular marker, experiments with transgenic mice overexpressing CCND1 proved that this protein alone cannot induce lymphomas (Hinds *et al.*, 1994; Lovec *et al.*, 1994), so that genomic aberrations other than the 11q13 translocation must be involved in the development and progression of MCL. To identify such additional aberrations, several studies using comparative genomic hybridization (CGH) and chromosome banding analyses have been conducted (Monni *et al.*, 1998; Beà *et al.*, 1999; Cuneo *et al.*, 1999; Bentz *et al.*, 2000; Bigoni *et al.*, 2001; Martinez-Climent *et al.*, 2001; Allen *et al.*, 2002). These studies showed that genomic imbalances, such as gain/amplification of 3q, 6p, 7p, 8q, 10p, 12q and 18q, and loss/deletion of 1p, 6q, 8p, 9p, 11q and 13q, frequently occur in MCL. Some genetic deregulations accompanying these genomic imbalances, such as *BMI-1* from amplification of 10p12.2, *p16^{INK4a}* from deletion of 9p21.3 and *ATM* from deletion of 11q22.3 (Dreyling *et al.*, 1997; Pinyol *et al.*, 1997; Stilgenbauer *et al.*, 1999; Schaffner *et al.*, 2000; Beà *et al.*, 2001; Rosenwald *et al.*, 2003), were also detected. However, the target genes of these other amplification and deletion sites remain unknown, one of the reasons being the limited resolution of chromosomal banding analysis or conventional CGH, which can detect only DNA copy number aberrations greater than 10–20 mega bases (Mb).

Recently, a chip-based CGH approach with high resolution and accuracy, known as array-based CGH (array CGH), was developed (Pinkel *et al.*, 1998). We established our own array CGH using a glass slide on which 2348 bacterial artificial chromosomes (BACs) and

P-1-derived artificial chromosomes (PACs) were spotted in duplicate with an average resolution of 1.3 Mb. In addition, our array CGH could identify a novel tumor-related gene, *C13orf25*, at 13q31.3 in B-cell lymphomas (Ota *et al.*, 2004). These results indicate that quantitative measurements of DNA copy number changes made with the array CGH can identify more accurately regions of genomic imbalance and that this procedure could thus be a useful tool for identification of tumor-related gene(s).

To gain a more accurate understanding of complex gene copy number changes and to identify key gain/loss regions in greater detail, we applied genome-wide array-based CGH to a panel of 29 patient samples and seven cell lines that derived from MCL.

Results

Genomic profiles of MCL patient samples and cell lines

Representative examples of the high-resolution analysis of a patient sample (G468) and SP-53 cell line are shown in Figure 1a and b, respectively. Array CGH could detect both small and whole-chromosome areas of gains and deletions as well as delineate amplification and deletion borders. A small amplicon involving clones containing known oncogenes was easily detected, as were small homozygous deletions.

Genomic imbalances of MCL patient samples

Gains or losses of genetic material shown by all 29 patient samples were subjected to data analysis. The entire tumor set involved copy number gains on an average of 130.6 Mb or 4.6%, and copy number loss on an average of 250.6 Mb or 8.8% of the genome. Total alterations averaged 3.8 regions of gain and 7.3 regions of loss. The genome-wide frequency of copy number alterations, both gains and losses, are shown in Figure 2. Regions of recurrent gain (≥five cases) involved chromosomes 3q13.11–q29, 6p21.32–p25.3, 7p14.3–p22.3, 8q13.2–q24.22, 10p12.1–p12.2 and 17q23.2–q24.1, and recurrent losses (≥five cases) localized at 1p36.23–p36.32, 1p11.2–p31.3, 1q42.2–q43, 2p11.2, 2q13, 5q21.1–q23.1, 6q16.2–q27, 8p12–p23, 9p24.3–q31.1, 10p12.31–p15.3, 11q14.3–q23.2, 13q13.2–q34, 15q13–q21.1, 17p11.2–p13.3, 19p13.2–p13.3 and 22q12.1–q13.1. The most frequent imbalances were gains of chromosomes 3q26.1 (48%), 7p21.1–p21.2 (34%), 6p25.3 (24%), 8q21.3–q24.21 (24%), 10p12.1–p12.2 (21%) and 17q23.2–q24.1 (17%), and losses of chromosome 2p11.2 (83%), 11q22.3–q23.1 (59%), 13q14.3–q21.1 (55%), 1p21.3–p22.1 (52%), 13q34 (52%), 9q22.33–q31.1 (45%), 17p13.3 (45%), 9p21.3–p22.1 (41%), 9p24.2–p24.3 (41%), 6q23.2–q24.1 (38%), 1p36.23–p36.32 (31%), 8p23.1–p23.3 (34%), 10p14–p15.3 (31%), 19p13.2 (28%), 5q22.1–q22.3 (21%), 22q12.2 (21%), 1q42.2–q43 (17%) and 2q13 (17%) (Table 1). Recurrent losses of 1p36.23–p36.32, 1q42.2–q43, 2p11.2, 2q13, 17p13.3 and 19p13.2–p13.3 were identified for the first time in this study,

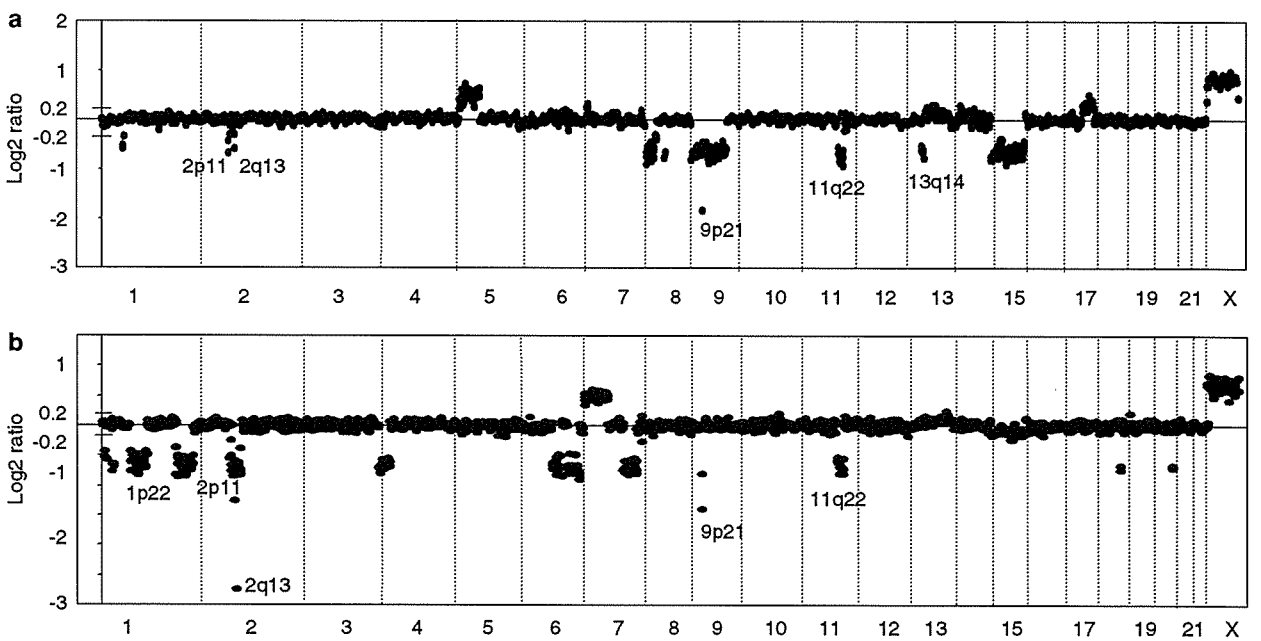

Figure 1 Representative genomic profiles for individual tumors. Whole genomic profiles are shown for a representative patient sample (**a**) and the SP-53 cell line (**b**). Log_2 ratios were plotted for all clones on the basis of chromosome position, with the vertical lines showing separation of chromosomes. The BACs and PACs are ordered according to their position in the genome from the 1p telomere on the left to the Xq telomere on the right. (**a**) Regions of copy number gain: 5p, 7p21.3, 17q21.31–q24.3 and X. Regions of copy number loss: 1p32, 2p11.2, 2q13, 8p12–p23.3, 8q12.3–q13.1, 9p24.3–q31.2, 11q22.3–q23.2, 13q14.3–q21.1 and 15. (**b**) Regions of copy number gain: 7p11.2–p22.3. Regions of copy number loss: 1p36.23–p36.32, 1p13.3–p31.2, 1q13.2–q44, 2p11.2–q14.3, 4p15.1–p16.1, 6q14.1–q21, 6q23.2–q26, 7q22.1–q32.3, 9p21.3–p22.1, 11q22.3–q23.2, 18q22.1 and 20q13.13–q13.2

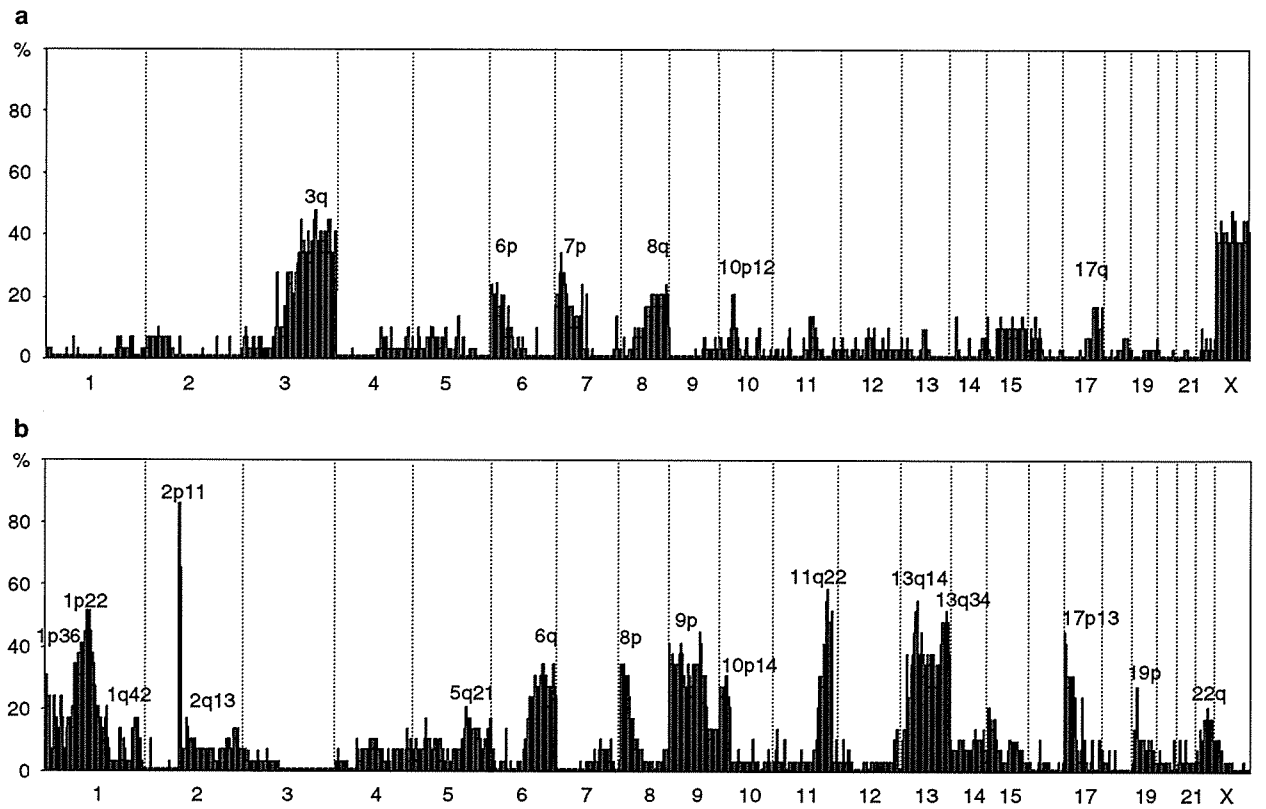

Figure 2 Genome-wide frequency of copy number alterations for 29 patients. (a) Frequency of copy number gains. (b) Frequency of copy number losses. Clones are ordered from chromosome 1 to 22 and within each chromosome according to their Sanger Center mapping position, May 2004 version

but no regions of gains were found other than those already listed in previous reports of studies using CGH for MCL.

Recurrent regions of high-level gains ($\log_2$ ratio $> +1.0$) were found at 10p12.2 (two cases, *BMI-1* gene locus), and recurrent regions of homozygous loss ($\log_2$ ratio < -1.0) at 2p11.2 (three cases, *Igκ* gene locus) and 9p21.1–p24.1. As shown in Table 2, the most frequently homozygously lost clone at 9p21–p24 was RP11-149I2 (five cases), which contains the $p16^{INK4a}$ tumor suppressor gene.

All the 59 clones on chromosome X were analysed separately because of sex mismatching, but the genomic alterations of X chromosomes were analysed only for the 17 male patients. Two cases showed low-grade copy number gains of Xq28, while three cases showed heterozygous (two cases) or homozygous (one case) loss of Xp21.3–p22.3 with the most frequent region at Xp22.31–p22.32.

Genomic imbalances of MCL cell lines

Genomic imbalances generally occurred more frequently in MCL cell lines than in patients. For example, gains of 7p21 and 8q24 (both $n=3$, 43%), and losses of 9p21 and 11q22 (both $n=6$, 86%), 1p22 ($n=5$, 71%) and of 6q, 8p23 and 13q21 (all $n=3$, 43%) were more frequently detected in MCL cell lines than in patient samples.

Recurrent regions of high-level gain were detected at 13q31.3 ($n=2$, *C13orf25* gene locus) and at 18q21 ($n=2$, *BCL2* gene locus).

Recurrent regions of homozygous loss were detected at 9p21.1–p24.1, 2p11.1 and 2q13 as seen in Table 2, which lists the homozygously lost clones of either patient samples or cell lines. Three cell lines (SP-53, Z-138 and Jeko-1) showed homozygous loss of 2q13 ($\log_2$ ratio < -1.0), while two (REC-1 and NCEB-1) showed heterozygous loss at 2q13 ($-1 \leqslant \log_2$ ratio $\leqslant -0.2$). Five patient samples with 2q13 deletion also displayed a heterozygous loss pattern. Individual partial genomic profiles of a patient sample (G468), and of cell lines SP-53, Z-138 and Jeko-1 of chromosome 2, are shown in Figure 3, which clearly indicates that the lowest locus of loss of 2q was at BAC, RP11-438K19 (BAC438K19), which contains two genes, *BIM* and *ACOXL* (Acyl-CoA dehydrogenase gene). The former is a BH3-only Bcl-2 family member protein that promotes apoptosis (O'Conner *et al.*, 1998), while the function of the latter remains unknown. As no information has been published regarding target gene(s) of homozygous loss at 2q13, we next searched for the minimum common region of loss of 2q13 to help us detect candidate target gene(s).

Table 1 Recurrent and most frequent regions of genomic gain and loss

Gain/loss	*Recurrent regions*[a]	*Most frequent regions*[b]				
	Chromosome[c]	*Chromosome*	*Mega base*[d] *(Mb)*	*No. of cases (%)*	*Clone*[e]	*Gene*[f]
	3q13.11–q29	3q26.1	162.6–170.1	13–14 (45–48%)	RP11–576M8	*SERPINI2*
		(3q27.1)	188.8	13 (45%)	RP11–211G3	*BCL6*
	6p21.32–p25.3	6p22.3–p25.3	0.4–24.6	5–7 (17–24%)	RP11–233K4	*IRF4*
Gain	7p14.3–p22.3	7p21.1–p21.3	8.7–19.8	9–10 (31–34%)	RP11–502P9	*HS7c218*
	8q13.2–q24.22	8q21.3–8q24.21	91.9–131.7	5–7 (17–24%)	RP1–80K22	*MYC*
	10p12.1–p12.2	10p12.1–p12.2	22.9–25.8	5–6 (17–21%)	RP11–301N24	*BMI-1*
	17q23.2–q24.1	17q23.2–q24.1	58.8–66.1	5 (17%)	RP11–51F16	
	1p36.23–p36.32	1p36.23–p36.32	2.5–7	8–9 (28–31%)	RP1–37J18	
	1p11.2–p31.3	1p21.3–p22.1	95.4–101.2	14–15 (48–52%)	RP4–561L24	*GCLM*
	1q42.2–q43	1q42.2–q43	230.9–238.2	5 (17%)	RP11–781K5	*Q8WUH8*
	2p11.2	2p11.2	89.4–89.9	19–24 (66–83%)	RP11–136K15	*KV1S(Igk)*
	2q13	2q13	108.7–111.9	5 (17%)	RP11–438K19	*BIM*
	5q21.1–q23.1	5q22.1–q22.3	104.8–114.5	5–6 (17–21%)	RP11–454E20	
	6q16.2–q27	6q23.2–q24.1	133.3–146.5	10–11 (34–38%)	RP11–356I2	*TNFAIP3*
	8p12–p23	8p23.1–p23.3	0.4–8.6	9–10 (31–34%)	RP11–240A17	
Loss	9p24.3–q31.1	9p24.2–p24.3	0.7–5.9	11–12 (38–41%)	RP11–130C19	
		9p21.3–p22.1	21.6–24	11–12 (38–41%)	RP11–149I2	*INK4a/ARF*
		9q22.33–q31.1	92.5–95.5	12–13 (41–45%)	RP11–54O15	*C9orf3*
	10p12.31–p15.3	10p14–p15.3	2.2–18.7	8–9 (28–31%)	RP11–401F24	*C10orf47*
	11q14.3–q23.2	11q22.3–q23.1	105–116.3	15–17 (52–59%)	RP11–758F15	*FDX*
		(11q22.3)	105–116.3	16 (55%)	RP11–241D13	*ATM*
	13q13.2–q34	13q14.3–q21.1	46–50.8	15–16 (52–55%)	RP11–364I19	*RFP2*
		13q34	99–112.5	13–15 (45–52%)	RP11–65D24	*bA65D24.2*
	15q13–q21.1	15q13.1	22.4–41	5–6 (17–21%)	RP11–125E1	
	17p11.2–p13.3	17p13.3	0.8–6.6	13 (45%)	RP11–676J12	*NXN*
		17p13.1	6.6–18.8	8–9 (28–31%)	RP11–199F11	*SP53*
	19p13.2–p13.3	19p13.2	6.4–7.9	7–8 (24–28%)	RP11–42J18	*CD202*
	22q12.1–q13.1	22q12.2	24.9–36.5	5–6 (17–21%)	RP1–76B20	*UCRX*

Region of gain or loss was defined as the contiguity of at least three clones showing gain or loss, or, if not contiguous, clones showing a high copy number gain ($\log_2$ ratio $> +1.0$) or a homozygous loss ($\log_2$ ratio < -1.0). [a]Recurrent region is defined as a region seen in $\geqslant 5$ of cases. [b]The most frequent region of gain/loss was defined as the region with the highest frequency within each recurrent region. [c]Regions are ordered according to their chromosomal position. [d]According to Sanger Center Institute, February 2004 version. [e]Representative of the most frequently gained or lost clone in each of the most frequent region. When the most frequently gained or lost clones share the same percentage of genomic aberrations in the most frequent regions, clones that include tumor-related genes are shown above those do not. [f]Genes contained in the representative clone

Table 2 List of BAC clones showing homozygous loss ($\log_2$ ratio < -1.0)

BAC name[a]	*Genes contained Clones*	*Cytogenetic position*	*Homozygous loss No. of patients* (n = 29)	*Homozygous loss No. of cell line* (n = 7)
RP11–136K15	*KV1S (Igk)*	2p11.2	3[b] (24)[d]	1[c] (6)[d]
RP11–438K19	*BIM*	2q13	0 (5)	3 (5)
RP11–77E14	*Q96GE9*	9p24.1	0 (10)	2 (4)
RP11–60C15	*PTPRD*	9p23	0 (10)	2 (4)
RP11–380P16	*IFNA5*	9p22.1	2 (11)	1 (5)
RP11–149I2	*INK4a/ARF*	9p21.3	5 (12)	3 (6)
RP11–214L15		9p21.3	2 (10)	0 (4)
RP11–393P6		9p21.3	2 (11)	1 (4)
RP11–337A23	*TEK*	9p21.2	2 (10)	0 (2)
RP11–205M20	*TAF1L*	9p21.1	2 (7)	0 (1)

[a]Clones are ordered according to their chromosomal position. [b]Number of patients showing homozygous loss in $\geqslant 2$ cases. [c]Number of cell lines showing homozygous loss. [d]Number of cases showing homozygous and heterozygous losses ($\log_2$ ratio < -0.2)

Southern blot analyses

To detect the target gene of 2q13 loss, we performed Southern blot analyses of seven MCL cell lines using six genomic probes, which were designed from the genomic DNA of BAC438K19 (Figure 4a). The analyses using probes 1–6 demonstrated that partial exons of *BIM* were commonly deleted in the three cell lines SP-53, Z-138 and Jeko-1, and that the 'minimum common region' of homozygous loss is the *BIM* but not the *ACOXL* gene locus (Figure 4b). Here, 'minimum common region' represents the portion of the region that is aberrant in MCL cell lines with aberrations in a region. The minimum common region of homozygous loss of 2q13

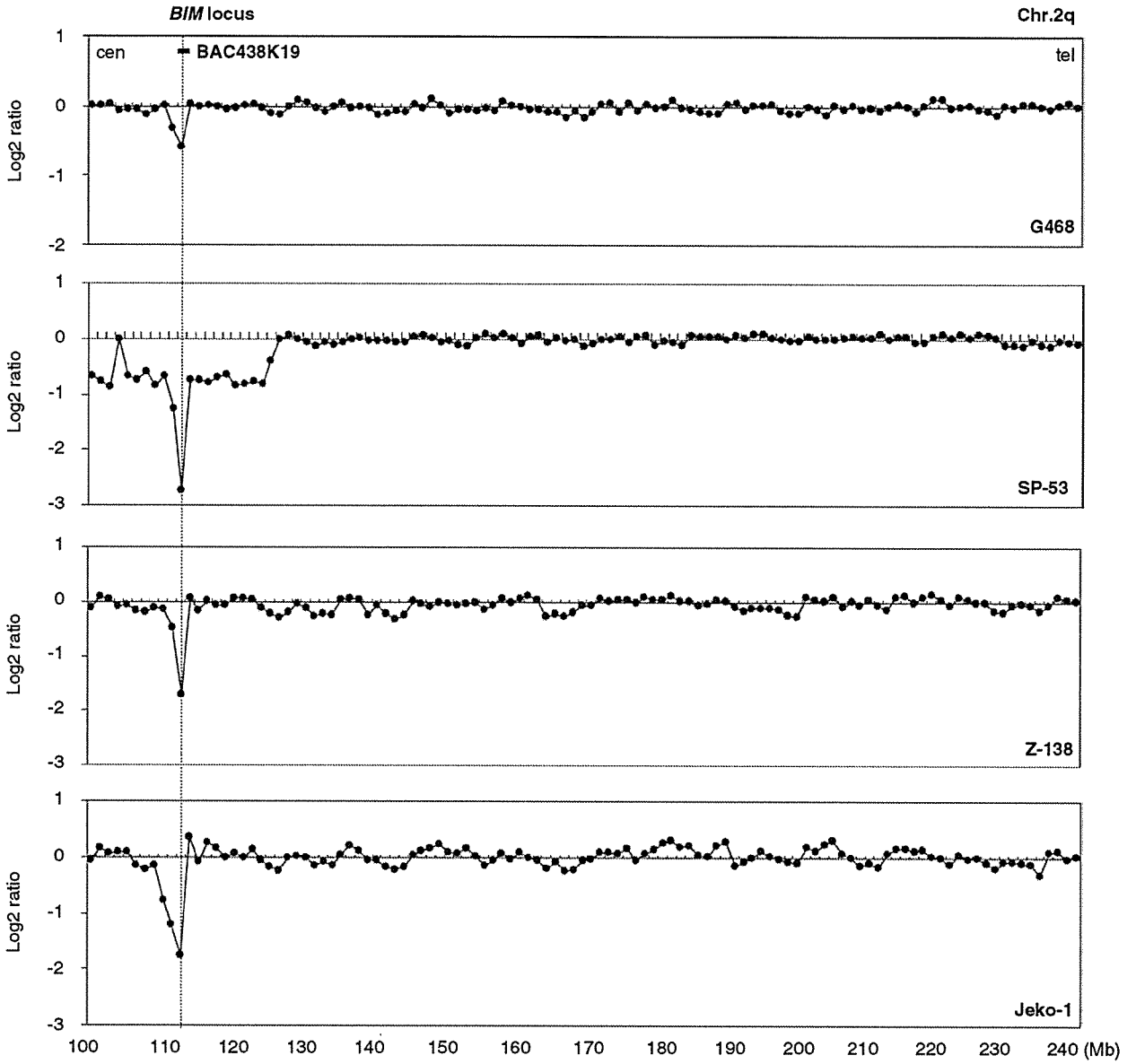

Figure 3 Genomic profiles of chromosome 2q from a patient sample (G468) and from three MCL cell lines (SP-53, Z-138 and Jeko-1). Log_2 ratio over +0.2 represents genomic copy number gain, and a log_2 ratio below −0.2 genomic copy number loss. Physical distances (Mb) from the 2q centromere are indicated. The vertical lines indicate the lowest locus of chromosome 2 at BAC438K19 containing the *BIM* gene. Log_2 ratios were −0.59 (G468), −2.75 (SP-53), −1.71 (Z-138) and −1.76 (Jeko-1) at BAC438K19, suggesting that homozygous loss occurs at the *BIM* gene locus

of these three cell lines ranges at least from probes 2 to 3 (15 kb) and at most from probes 1 to 4 (45 kb). This region includes the open reading frame of *BIM* but no other gene according to the NIBC, Ensembl Genome Data Resources and UCSC Genome Bioinfomatics. Southern blot analyses were also performed with probes from BAC, RP11-368A17 (probe 7) and BAC, RP11-537E18 (probe 8) for seven MCL cell lines. BAC, RP11-368A17 (BAC368A17) is a clone with a 1.55 Mb telomeric to BAC438K19, and BAC, RP11-537E18 (BAC537E18) a clone with a 1.85 Mb centromeric to BAC438K10. Bands of probes 7 and 8 were positive in all seven MCL cell lines (data not shown), indicating that the region of homozygous deletion of each cell line (SP-53, Z-138 and Jeko-1) is at a maximum of 3.4 Mb.

Furthermore, we performed Southern blot analysis of patient samples for which materials were available (Figure 5a), and found a heterozygous deletion pattern in a patient sample (G468) that showed heterozygous deletion at 2q13.

Northern blot analysis

To examine the expression of *BIM* in MCL cell lines, Northern blot analysis was performed of seven MCL

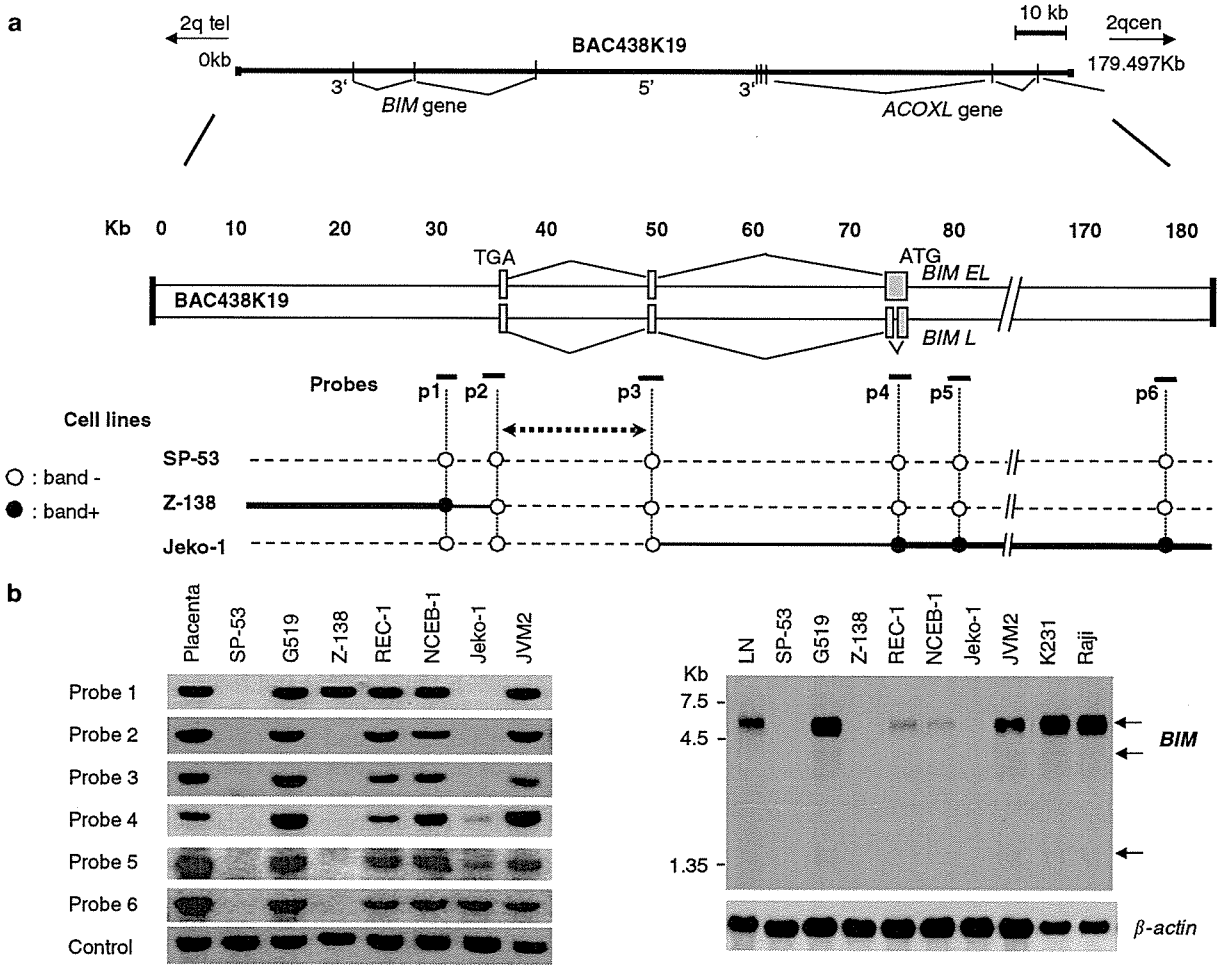

Figure 4 Minimum common region of homozygous loss at 2q13 and expression of *BIM*. (**a**) Schematic illustration of BAC438K19, the *BIM* gene exons, and loss patterns of three cell lines (SP-53, Z-138 and Jeko-1). Gray boxes: exons (open reading frames) of *BIM EL* and *BIM L*. The open reading frame of *BIM EL* (597 bp) consists of three exons: exon 1 from 75 082 to 75 475 bp (394 bp) including the initiating codon (ATG), exon 2 from 49 074 to 49 177 bp (104 bp), and exon 3 from 34 990 to 35 088 bp (99 bp) including the termination codon (TGA), all on BAC438K19. Black and white circles: probes used for Southern blot analyses. Broken horizontal lines with white circles: homozygous loss (bands negative). Thick horizontal lines with black circles: no homozygous loss (bands positive). Thin horizontal lines: not confirmed whether homozygous loss or not. Bold broken horizontal arrows between probes 2 and 3 indicate the minimum common region of homozygous loss of 2q13. (**b**) Southern blot analyses using probes 1–6 for genomic DNAs of MCL cell lines. Lane 1, human placenta; lane 2, SP-53; lane 3, Granta 519 (G519); lane 4, Z-138; lane 5, REC-1; lane 6, NCEB-1; lane 7, Jeko-1; lane 8, JVM2. Bands of probe 1: human placenta (+), SP-53 (−), Granta 519 (+), Z-138 (+), REC-1 (+), NCEB-1 (+), Jeko-1 (−), and JVM2 (+). Bands of probes 2 and 3: human placenta (+), SP-53 (−), Granta 519 (+), Z-138 (−), REC-1 (+), NCEB-1 (+), Jeko-1 (−), and JVM2 (+). Bands of probe 4: human placenta (+), SP-53 (−), Granta 519 (+), Z-138 (−), REC-1 (+), NCEB-1 (+), Jeko-1 (+/−), and JVM2 (+). Bands of probes 5 and 6: human placenta (+), SP-53 (−), Granta 519 (+), Z-138 (−), REC-1 (+), NCEB-1 (+), Jeko-1 (+), and JVM2 (+). 'Control' indicates the representative control band of probe 3 (TCR β probe) located under the bands of probe 6. (**c**) Northern blot analysis of *BIM* with seven MCL cell lines, B-cell lymphoma (Karpas 231) and Burkitt's lymphoma (Raji) cell lines. Control is β-actin

cell lines, one FCL cell line (Karpas 231) and one Burkitt's cell line (Raji). As shown in Figure 4c, three transcripts of *BIM*, one major (5.7 kb) and two minor (3.8 kb and 1.35 kb) bands, were observed in Granta 519, JVM2, Karpas 231 and Raji, whereas no or very weak expression was detected in SP-53, Z-138, Jeko-1, REC-1 and NCEB-1. Although array CGH data showed a heterozygous pattern at 2q13 in REC1 and NCEB1 cell lines, Northern blot analysis indicated that BIM mRNA in these two cell lines was clearly down-regulated, which will be the result of a gene dosage effect.

Fluorescence in situ *hybridization (FISH)*

Dual-color FISH using a combination of BAC438K19 and BAC368A17 (1.55 Mb telomeric to BAC438K19) and one of BAC438K19 and BAC537E18 (1.85 Mb centromeric to BAC 438K10) was performed on three MCL cell lines (SP-53, Z-138 and Jeko-1) and a patient

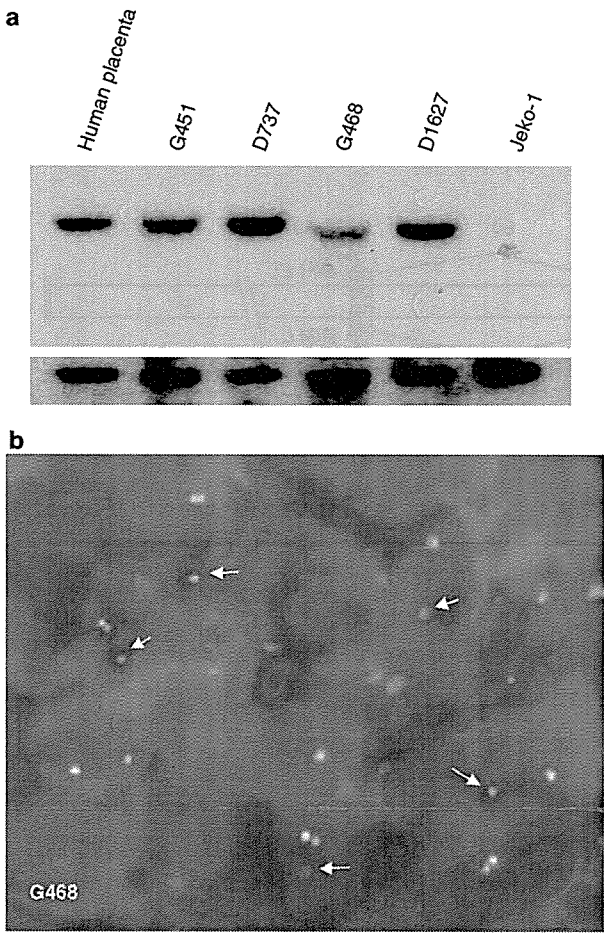

Figure 5 Southern blot and FISH analysis of a patient sample (G468). (**a**) Southern blot analysis. Lane 1: human placenta. Lanes 2, 3, 5: Patient samples without 2q13 deletion. Lane 4: G468 showing 2q13 loss by array CGH (see Figure 3). Lane 6: Jeko-1 cell line showing homozygous deletion at *BIM* locus. Probe 2 that contain *BIM* exon was used in this experiment. (**b**) Dual-color FISH analysis with probes A and B of G468. Probe A: BAC438K19; probe B: BAC368A17. Probe B is 1.55 Mb telomeric to probe A, and BAC438K19 contains the *BIM* gene. Interphase chromosomes have two pairs of red signals (probe B, red), and one pair of green signals (probe A, green), indicating heterozygous loss of probe A

sample (G468). These three clones were placed contiguously on our array CGH glass slide. Results of dual-color FISH analysis using BAC438K19 and BAC368A17 for the patient sample (G468) are shown in Figure 5b. FISH results for these cell lines (data not shown) correlated well with the array CGH data. (i) In the SP-53 cell line, no signal of BAC438K19 was found, whereas two pairs of BAC368A17 signals, or one pair of BAC537E18 signals was observed, indicating homozygous deletion of the BAC438K19 clone ($\log_2$ ratio $= -2.74$). (ii) In the Z-138 cell line, one pair of weak BAC438K19 signals was detected but two pairs of normal BAC368A17 signals or one pair of normal BAC537E18 signals was observed, suggesting intra-BAC438K19 deletion in this cell line ($\log_2$ ratio $= -1.71$). (iii) In the Jeko-1 cell line, one pair of weak BAC438K19 signals but two pairs of normal BAC368A17 signals or one pair of weak BAC537E18 signals was observed, suggesting the deletion of intra-BAC438K19 in this cell lines ($\log_2$ ratio $= -1.76$). These observations are concordant with the finding of total BAC438K19 deletion in SP-53 and partial BAC438K19 homozygous deletion in the Z-138 and Jeko-1 cell lines.

Discussion

In the study reported here, high-resolution mapping of copy number changes was achieved for the entire MCL genome. Frequent gains and losses could be identified with high resolution by means of array analysis, which allows for precise mapping of genomic aberrations. Although numerous genomic changes of MCL were identified by array CGH, many of them were the same as those previously listed in reports of studies using chromosomal CGH (also known as conventional CGH). Several authors (Monni *et al.*, 1998; Beà *et al.*, 1999; Bentz *et al.*, 2000; Martinez-Climent *et al.*, 2001; Allen *et al.*, 2002) reported recurrent regions of gain as 3q (40–70%), 6p (20%), 7p (27%), 8q (20–30%), 10p (20%), 12q (20–30%), 18q21 (20%) and recurrent regions of loss as 1p (24–33%), 6q (27–37%), 8p (20–30%), 9p (16–30%), 11q (22–30%) and 13q (40–60%). However, the incidence of genomic aberrations identified by array CGH was generally higher than that reported in chromosomal CGH studies. For example, our data show more frequent losses of 1p21–p22 (52%) and 9p21 (41%, *INK4/ARF* locus), as well as of 11q22 (55%, *ATM* locus), than the corresponding losses previously detected by chromosomal CGH. Among these frequent losses, although the candidate target gene of 1p22 loss could not be identified, our array CGH analysis showed a most frequent region of loss within the 5.8 Mb region of 1p21.3–p22.1.

Recently, Kohlhammer *et al.*, 2004 reported the results of their study of 49 patients for which they used array-based (matrix) CGH with glass slides on which 812 artificial chromosomes were spotted, and found higher frequencies of genomic alterations of MCL than those seen in chromosomal CGH data. Their patient characteristics (e.g. percentage of stage III/IV, poor performance status, high LDH level, leukemic MCL and extra-nodal involvement) were almost the same as those of our series, as were the frequencies of genomic alterations. However, they could not identify several regions of loss detected by us, such as 1p36, 1q42.2–q43, 2p11.2, 2q13, 17p13.3 and 19p13.2–p13.3, because their clones were not selected from throughout the genome. The superior resolution of our study can thus be attributed to the unbiased selection of artificial chromosome clones from throughout the genome.

Of the six novel genomic regions of loss detected in our study, loss of 17p13.3 deserves special comment because it is highly interesting in that our array CGH analysis of 17p showed the most frequently deleted region(s) at 17p13.3, which suggests the existence of an additional tumor suppressor gene(s) distal to the *SP53* gene. Frequent allelic loss at 17p13.3 independent of the

SP53 locus has also been found in a variety of other human malignancies including lung, breast, ovarian and hepatocellular carcinomas as well as neural tumors (Fujimori *et al.*, 1991; Cogen *et al.*, 1992; Saxena *et al.*, 1992; Phillips *et al.*, 1996; Schultz *et al.*, 1996; Konishi *et al.*, 2002). Although *SP53* mutation in MCL is a well-known genomic alteration and is associated with variant cytology and poor prognosis (Greiner *et al.*, 1996; Hernandez *et al.*, 1996), our finding indicated that other candidate tumor suppressor gene(s) at 17p13.3 may also be involved in the lymphomagenesis of MCL.

The key biological value of high-resolution array CGH lies in its ability to detect small, high-level gains in copy numbers and homozygous deletions that are capable of harboring specific oncogenes and tumor suppressor genes. Recurrent regions of high-level copy number gains have been identified as 10p12.2 (*BMI-1*), 13q31.3 (*C13orf25*) and 18q21 (*BCL2*) (Beà *et al.*, 2001; Hofmann *et al.*, 2001; Martínez *et al.*, 2003; Ota *et al.*, 2004). Since biallelic (homozygous) loss is considered to be a hallmark of chromosomal regions harboring tumor suppressor genes (Knudson, 1971), the detection of recurrent regions of homozygous loss at 2p11, 2q13 and 9p21–p24 is significant. Loss of 2p11 may be due to immunoglobulin gene rearrangement, but the loss region of 9p21–p24 covers nearly 15 Mb, making it difficult to identify the responsible gene(s) even though this region features the most frequently and homozygously deleted clone, RP11-149I2, which contains the $p16^{INK4a}$ gene, which may well be the candidate gene for this region of homozygous loss of MCL (Dreyling *et al.*, 1997; Pinyol *et al.*, 1997).

While no previous studies have reported any candidate target gene of 2q13 among the three homozygous loss regions, our study showed that the minimum common region of 2q13 loss contains partial exons of *BIM* but no other genes or ESTs. This suggests that *BIM* appears to be the most likely target of this region of loss. It has recently become known that disturbances of pathways associated with apoptosis also contribute to the development of MCL (Hofmann *et al.*, 2001; Martínez *et al.*, 2003). Another study found that *BIM* is a proapoptotic *BCL2* family member and a major physiological antagonist of BCL2, particularly in hematopoietic systems (Bouillet *et al.*, 2002), and Enders *et al.* (2003) recently reported that B lymphocytes lacking Bim are refractory to apoptosis induced by B-cell receptor ligation *in vitro*. Finally, Egle *et al.* (2004) using $Bim^{-/-}$ and $Bim^{+/-}$ Eμ-*Myc* mice, demonstrated that the loss of *Bim* was related to the onset of oncogenesis. These findings strongly suggest that *BIM* could be a tumor suppressor gene.

We demonstrated that the minimum common region of loss of 2q13 in MCL cell lines occurred at the *BIM* locus. Furthermore, we confirmed that the *BIM* expression of five out of seven MCL cell lines was downregulated, while normal expression was found in two MCL cell lines without deletion of 2q13. These results constitute a powerful indication that *BIM* is the most likely candidate target gene of 2q13 loss/deletion and that its down-regulation may contribute to tumorigenesis of MCL.

In summary, the use of high-resolution array CGH technology for a detailed study of MCL allowed for an accurate identification of genomic aberrations and identification of *BIM* as a possible novel candidate tumor suppressor in MCL.

Materials and methods

MCL patients and samples

Tumor specimens obtained from 29 MCL cases, comprising 16 males and 13 females all from the Aichi Cancer Center, were included in the study. In all, 24 cases were classified as typical and five as blastoid variants. The median age of the patient was 67 years (49–92 years old). Out of 27 cases, 18 (67%) were leukemic (data of 27 cases were available), 27 out of 29 cases (93%) were in an advanced stage III–IV, eight out of 27 cases (30%) had elevated LDH (data of 27 cases were available), five out of 28 cases (18%) had a poor performance status (data of 28 cases were available) and 21 out of 27 cases (78%) had more than one extranodal site of involvement (data of 27 cases were available). The immunophenotype of the tumors was determined by immunohistochemistry for tissue sections and/or flow cytometry for cell suspensions. These studies used Ig light and heavy chains, several B-cell (CD19, CD20, CD22, CD45RA and CD79a) and T-cell (CD2, CD3, CD5, CD7, CD4, CD8, CD45RO and CD43) markers, CD10 and CD23. CCND1 expression was examined in all cases by Northern blot analysis and/or immunohistochemistry (Suzuki *et al.*, 1999). All tumors included in this study had a B-cell phenotype, co-expressed CD5 and showed CCND1 overexpression.

MCL cell lines

The seven MCL-derived cell lines used were SP-53, Granta 519, Z-138, REC-1, NCEB-1, Jeko-1 and JVM2. All these MCL cell lines have been thoroughly characterized in terms of morphology, immunophenotype and/or interphase cytogenetics (detection of t(11;14)(q13;q32)) (Saltman *et al.*, 1988; Jeon *et al.*, 1998; Amin *et al.*, 2003). The JVM2 cell line, derived from a prolymphocytic leukemia and carrying t(11;14)(q13;q32), was also included in the study. Z-138, NCEB-1, Granta 519, REC-1 and JVM2 were kindly provided by Dr Martin Dyer of Leicester University, UK. Karpas 231 derived from follicular lymphoma (FCL) and carrying t(14;18)(q32;q21) was kindly provided by Dr Abraham Karpas of the Medical Research Council Center, Hills Road, Cambridge, UK (Nacheva *et al.*, 1993). The Raji cell line was derived from Burkitt's lymphoma.

DNA and RNA samples

High molecular weight DNA was extracted from 29 lymph nodes using standard Proteinase K/RNAse treatment and phenol–chloroform extraction. Normal DNA was obtained from male and healthy blood donors. RNAs were prepared from cell lines by homogenization in guanidinium thiocyanate and centrifugation through cesium chloride.

Array-based CGH

The array consisted of 2348 BAC and PAC clones, covering the human genome at a resolution of roughly 1.3 Mb, from libraries RP11 and RP13 for BAC clones, and RP1, RP3, RP4 and RP5 for PAC clones. BAC and PAC clones were selected from the information in NCBI (http://www.ncbi.nlm.nih.gov/), Ensembl Genome Data Resources (http://www.ensembl.org/) and UCSC

genome Bioinfomatics (http://www.ncbi.nlm.nih.gov/), and obtained from the BACPAC Resource Center at the Children's Hospital (Oakland Research Institute, Oakland, CA, USA). Clones were ordered from chromosomes 1 to 22 and X within each chromosome on the basis of Ensembl Genome Data Resources from the Sanger Center Institute, February 2004 version. The locations of all the clones used for array CGH were confirmed by fluorescence *in situ* hybridization (FISH). Clone names and their chromosome locations are available on request. The template for degenerate oligonucleotide-primed PCR (DOP-PCR) consisted of 10 ng of BAC (or PAC) DNA. DOP-PCR products were ethanol precipitated and dissolved in DNA spotting solution DSP0050 (Matsunami, Osaka, Japan) and robotically spotted in duplicate onto CodeLink™ activated slides (Amersham Biosciences, Piscataway, NJ, USA) using the inkjet technique by a ceramic actuator (NGK, Nagoya, Japan). Fabrication and validation of the array, hybridization methods and analytical procedures have been described elsewhere in detail (Ota *et al*., 2004). Briefly, 1 μg of tested (tumor or normal) and of referenced (normal) DNA was digested with *Dpn*II and labeled with the BioPrime DNA labeling system (Invitrogen Life Technologies, Inc., Tokyo, Japan) using Cy3-dUTP and Cy5-dUTP (Amersham Pharmacia Biotech, Piscataway, NJ, USA) for the tested and referenced DNA, respectively. Test and reference DNAs were then mixed with 100 μg of Cot-1 DNA (Life Technologies, Inc., Gaithersburg, MD, USA), precipitated and resuspended in 45 μl of a hybridization solution (50% formamide, 10% dextran sulfate, 2 × SCC, 4% SDS and 100 μg tRNA) and hybridized onto a glass slide. After 48–66 h hybridization, the slide was washed and scanned with an Agilent Micro Array Scanner (Agilent Technologies, Palo Alto, CA, USA) and the acquired array images were analysed with Genepix Pro 4.1 (Axon Instruments, Inc., Foster City, CA, USA). After automatic segmentation of the DNA spots and subtraction of the local background, intensities of the signals were determined. Subsequently, ratios of the signal intensity of two dyes (Cy3 intensity/Cy5 intensity) were calculated for each spot and converted into $\log_2$ ratios on an Excel sheet in the order of chromosomal position. For the array, six simultaneous hybridizations of normal male versus normal male were performed to define the normal variation for the $\log_2$ ratio. A total of 113 clones with less than 10% of the mean fluorescence intensity of all the clones, with the most extreme average test over reference ratio deviations from 1.0 and with the largest s.d. in this set of normal controls were excluded from further analyses. Thus, we analysed a total of 2235 clones (covered 2988 Mb, 1.3 Mb of resolution) for further analysis. Out of 2235, 2176 clones (covered 2834 Mb) were from chromosome 1p telomere to 22q telomere. 59 out of 2235 clones were from chromosome X. Since more than 96% of the measured fluorescence $\log_2$ ratio values of each spot (2 × 2235 clones) ranged from +0.2 to −0.2, the thresholds for the $\log_2$ ratio of gains and losses were set at the $\log_2$ ratios of +0.2 and −0.2, respectively. Regions of low-level gain/amplification were defined as $\log_2$ ratio +0.2 to +1.0, those suggested of containing a heterozygous loss/deletion as $\log_2$ ratio −1.0 to −0.2, those showing high-level gain/amplification as $\log_2$ ratio > +1.0, and those suggested of containing a homozygous loss/deletion as $\log_2$ ratio <−1.0.

Southern blot analyses

To detect the target gene of 2q13 loss, probes 1–6 were designed from genomic DNA on BAC 438K19. The length of BAC 438K19 (Accession number: AC096670) is 179 497 bp. Probes 7 and 8 were designed from genomic DNA on BAC 368A17 (1.55 Mb telomeric to BAC438K19) and BAC537E18 (1.85 Mb centromeric to BAC 438K19), respectively. Probes 1–8 used by Southern blot analysis were amplified with the PCR method using eight primer pairs from human placenta DNA. The primer pairs used for PCR were Probe 1 (850 bp): sense (BAC438K19: 30 851–30 874 bp), 5′-ttgcacaagtaaagtggcaattac-3′; antisense (BAC438K19: 31 700–31 677 bp), 5′-atccctgacaactcagcgtttaga-3′, Probe 2 (837 bp): sense (BAC438K19: 34 214–34 237 bp), 5′-acgaatggttatcttacgactgtt-3′; antisense (BAC438K19: 35 050–35 027 bp), 5′-atctatgcatctgagtccagactg-3′, Probe 3 (850 bp): sense (BAC438K19: 49 071–49 094 bp), 5′-taccctccttgcatagtaa gcgtt-3′; antisense (BAC438K19: 49 920–49 897 bp), 5′-tagtgacag cttaatgaaagggca-3′, Probe 4 (811 bp): sense (BAC438K19: 75 127–75 150 bp), 5′-gggtttgtgttgatttgtcacaac-3′; antisense (BAC438K19: 75 937–75 914 bp), 5′-tgctgccctcagcattttcggcaa-3′, Probe 5 (1095 bp): sense (BAC438K19: 80 501–80 524 bp), 5′-ggg tttgtgtt gatttgtcacaac-3′; antisense (BAC438K19: 81 595–81 572 bp), 5′-cc gcgctggagttacaaactctat-3′ and Probe 6 (890 bp): sense (BAC438K19: 177 361–177 384 bp), 5′-cattccccagaaacagatctcgtt-3′; antisense (BAC438K19: 178 250–178 227 bp), 5′-catagcattat-caatgccatcgat-3′. Probe 7 (820 bp): sense (BAC368A17: 34 301–34 320 bp), 5′-ccatagttaatgtacacagc-3′; antisense (BAC368A17: 35 101–35 120 bp), 5′-tcgcaaaccattagga actg-3′. Probe 8 (500 bp): sense (BAC537E18: 191 071–191 094 bp), 5′-ttggagccaaggtaggat-taaaca-3′; antisense (BAC537E18: 191 487–191 570 bp), 5′-ctggag-gaatagtgcttccagatg-3′. Probes 2–4 included an open reading frame of *BIM*. *BIM* (*BIM EL*) has several splice variants such as *BIM L*, *BIM* alpha, *BIM* beta and *BIM* gamma (O'Connor *et al*., 1998; U *et al*., 2001; Liu *et al*., 2002), and the open reading frame of *BIM EL* (597 bp) includes exons of these variants. Probe 4 includes the initiating codon (ATG) of *BIM* (*BIM EL* and *BIM L*), and Probe 2 the termination codon (TGA) of *BIM*. Amplifications were performed on a Thermal Cycler (Perkin-Elmer Corporation, Norwalk, CT, USA). PCR was conducted with the touchdown PCR method described elsewhere (Motegi *et al*., 2000). Briefly, the reactions consisted of 10 cycles of denaturation (94°C, 0.5 min), annealing (63°C, 0.5 min, 1°C decrease per two cycles), and extension (72°C, 2.5 min), followed by 25 cycles of denaturation (94°C, 0.5 min), annealing (58°C, 0.5 min), and extension (72°C, 2.5 min), and a final extension of 5 min at 72°C. The basic annealing temperature of the reaction ranged from 63 to 58°C. All PCR products were separated by electrophoresis and purified with the QIA Quick™ Gel Extraction Kit (Qiagen). TA cloning to purified PCR products was performed with the aid of pBluescriptII SK (−), and sequenced with the ABI PRISM™ 310 Genetic Analyzer (Applied Biosystems, Foster City, VA, USA). In all, 10 μg of each genomic DNA sample was restriction digested for 16 h with *Bam*H1 (for probes 1 and 6) or *Hin*dIII (for probes 2–4) and electrophoresed on a 0.8% agarose gel in 1 × TBE. Gels were sequentially immersed in 0.25 M HCl for 30 min, 1.5 M NaCl/0.5 M NaOH for 30 min and 0.5 M Tris (pH 7.4)/1.5 M NaCl for 30 min. Electrophoresed DNA was then transferred onto Hybond N^+ membranes (Amersham Pharmacia Biotech, Tokyo, Japan), washed and hybridized overnight at 65°C with [α-^{32}P]-dCTP-labeled probes 1–8. It was then washed, first with 2 × SSC and then with diminishing concentrations of SSC-0.1% *N*-lauryl sarcosine at 65°C, and finally exposed to BioMax™ MS films (EKC, Rochester, NY, USA).

Northern blot analysis

Northern blotting was performed with *BIM EL* cDNA against seven MCL cell lines, Karpas 231 (FCL) and Raji (Burkitt's lymphoma). Probes used for Northern blot analysis were amplified with the RT–PCR method using a primer pair: sense, 5′-atggcaaagcaaccttctgatgta-3′; antisense, 5′-tcaatgcattctccacac-caggcg-3′. cDNA (open reading frame, 597 bp) of *BIM EL* was

generated from fetal brain cDNA. Total cellular RNA (10 μg) was size-fractioned on a 1% agarose/0.66 M formaldehyde gel and transferred onto a Hybond-N$^+$ nylon membrane (Amersham Pharmacia Biotech, Tokyo, Japan). The membranes were then hybridized overnight at 42°C with [α-^{32}P]-dCTP-labeled probes, washed and finally exposed to BioMax™ MS films.

Fluorescence in situ *hybridization*

Interphase chromosomes were prepared from paraffin-embedded sample (G468) and cell lines. Dual-color FISH analysis was conducted as described previously (Nomura *et al.*, 2003; Zhang *et al.*, 2004). Probes used in this experiment were probe A: BAC438K19 (green) and probe B: BAC368A17 (red).

Acknowledgements
The outstanding technical assistance of Ms H Suzuki and Y Kasugai is very much appreciated. We also wish to thank Dr Ryuzo Ohno, the chancellor of Aichi Cancer Center, for his general support. This work was supported in part by a Grant-in-Aid from the Ministry of Health, Labour and Welfare, a Grant-in-Aid from the Ministry of Education, Culture, Sports, Science and Technology, a Grant-in-Aid (B2) from the Japan Society for the Promotion of Science, a Grant-in-Aid from the Foundation of Promotion of Cancer Research, a Grant-in-Aid for Cancer Research from the Princess Takamatsu Cancer Research Fund and a Grant-in-Aid from the China Japan Medical Association.

References

Allen JE, Hough RE, Goepel JR, Bottomley S, Wilson GA, Alcock HE, Baird M, Lorigan PC, Vandenberghe EA, Hancock BW and Hammond DW. (2002). *Br. J. Haematol.*, **116,** 291–298.

Amin HM, McDonnell TJ, Medeiros LJ, Rassidakis GZ, Leventaki V, O'Connor SL, Keating MJ and Lai R. (2003). *Arch. Pathol. Lab. Med.*, **127,** 424–431.

Beà S, Ribas M, Hernández JM, Bosch F, Pinyol M, Hernández L, García JL, Flores T, González M, López-Guillermo A, Piris MA, Cardesa A, Montserrat E, Miró R and Campo E. (1999). *Blood*, **93,** 4365–4374.

Beà S, Tort F, Pinyol M, Puig X, Hernández L, Hernández S, Fernández PL, Lohuizen M, Colomer D and Campo E. (2001). *Cancer Res.*, **61,** 2409–2412.

Bentz M, Plesch A, Bullinger L, Stilgenbauer S, Ott G, Muller-Hermelink HK, Baudis M, Barth TF, Moller P, Lichter P and Dohner H. (2000). *Genes Chromosomes Cancer*, **27,** 285–294.

Bigoni R, Cuneo A, Milani R, Roberti MG, Bardi A, Rigolin GM, Cavazzini F, Agostini P and Castoldi G. (2001). *Leuk. Lymphoma.*, **40,** 581–590.

Bouillet P, Purton JF, Godfrey DI, Zhang LC, Coultas L, Puthalakath H, Pellegrini M, Cory S, Adams JM and Strasser A. (2002). *Nature*, **415,** 922–926.

Cogen PH, Daneshvar L, Metzger AK, Duyk G, Edwards MS and Sheffield VC. (1992). *Am. J. Hum. Genet.*, **50,** 584–589.

Cuneo A, Bigoni R, Rigolin GM, Roberti MG, Bardi A, Piva N, Milani R, Bullrich F, Veronese ML, Croce C, Birg F, Dohner H, Hagemeijer A and Castoldi G. (1999). *Blood*, **93,** 1372–1380.

Dreyling MH, Bullinger L, Ott G, Stilgenbauer S, Muller-Hermelink HK, Bentz M, Hiddemann W and Dohner H. (1997). *Cancer Res.*, **57,** 4608–4614.

Egle A, Harris AW, Bouillet P and Cory S. (2004). *Proc. Natl. Acad. Sci. USA*, **101,** 6164–6169.

Enders A, Bouillet P, Puthalakath H, Xu Y, David M, Tarlinton DM and Strasser A. (2003). *J. Exp. Med.*, **198,** 1119–1126.

Fujimori M, Tokino T, Hino O, Kitagawa T, Imamura T, Okamoto E, Mitsunobu M, Ishikawa T, Nakagama H, Harada H, Yagura M, Matsubara K and Nakamura Y. (1991). *Cancer Res.*, **51,** 89–93.

Greiner TC, Moynihan MJ, Chan WC, Lytle DM, Pedersen A, Anderson JR and Weisenburger DD. (1996). *Blood*, **87,** 4302–4310.

Hernandez L, Fest T, Cazorla M, Teruya-Feldstein J, Bosch F, Peinado MA, Piris MA, Montserrat E, Cardesa A, Jaffe ES, Campo E and Raffold M. (1996). *Blood*, **87,** 3351–3359.

Hinds PW, Dowdy SF, Eaton EN, Arnold A and Weinberg RA. (1994). *Proc. Natl. Acad. Sci. USA*, **91,** 709.

Hofmann W-K, de Vos S, Tsukasaki K, Wachsman W, Pinkus GS, Said JW and Koeffler P. (2001). *Blood*, **98,** 787–794.

Jaffe ES (ed). (2001). *World Health Classification of Tumors: Pathology & Genetics of Tumours of Haematopoietic and Lymphoid Tissues.* IARC Press: Lyon and Washington.

Jeon HJ, Kim CW, Yoshino T and Akagi T. (1998). *Br. J. Haematol.*, **102,** 1323–1326.

Knudson Jr AG. (1971). *Proc. Natl. Acad. Sci. USA*, **68,** 820–823.

Kohlhammer H, Schwaenen C, Wessendorf S, Holzmann K, Kestler HA, Kienle D, Barth T, Moller P, Ott G, Kalla J, Radlwimmer B, Pscherer A, Stilgenbauer S, Dohner H, Lichter P and Bentz M. (2004). *Blood*, **104,** 795–801.

Konishi H, Nakagawa T, Harano T, Mizuno K, Saito H, Masuda A, Matsuda H, Osada H and Takahashi T. (2002). *Cancer Res.*, **62,** 271–276.

Liu J-W, Chandra D, Tang S-H, Chopra D and Tang DG. (2002). *Cancer Res.*, **62,** 2976–2981.

Lovec H, Grzeschiczek A, Kowalski B and Moroy T. (1994). *EMBO J.*, **13,** 3487–3495.

Martinez-Climent JA, Vizcarra E, Sanchez D, Blesa D, Rubio-Moscardo F, Albertson DG, Garcia-Conde J, Dyer MJS, Levy R, Pinkel D and Lossos IS. (2001). *Blood*, **98,** 3479–3482.

Martínez N, Camacho FI, Algara P, Rodríguez A, Dopazo A, Ruíz-Ballesteros E, Martín P, Martínez-Climent JA, García-Conde J, Menárguez J, Solano F, Mollejo M and Piris MA. (2003). *Cancer Res.*, **63,** 8226–8232.

Monni O, Oinonen R, Elonen E, Franssila K, Teerenhovi L, Joensuu H and Knuutila S. (1998). *Genes Chromosomes Cancer*, **21,** 298–307.

Motegi M, Yonezumi M, Suzuki H, Suzuki R, Hosokawa Y, Hosaka S, Kodera Y, Morishima Y, Nakamura S and Seto M. (2000). *Am. J. Pathol.*, **156,** 807–812.

Nacheva E, Dyer MJ, Fischer P, Stranks G, Heward JM, Marcus RE, Grace C and Karpas A. (1993). *Blood*, **82,** 231–240.

Nomura K, Yoshino T, Nakamura S, Akano Y, Tagawa H, Nishida K, Seto M, Nakamura S, Ueda R, Yamagishi H and Taniwaki M. (2003). *Cancer Genet. Cytogenet.*, **140,** 49–54.

Ota A, Tagawa H, Karnan S, Karpas A, Kira S, Yoshida Y and Seto M. (2004). *Cancer Res.*, **64,** 3087–3095.

O'Connor L, Strasser A, O'Reilly LA, Hausmann G, Adams JM, Cory S and Huang DC. (1998). *EMBO J.*, **17,** 384–395.

Phillips NJ, Ziegler MR, Radford DM, Fair KL, Steinbrueck T, Xynos FP and Donis-Keller H. (1996). *Cancer Res.*, **56,** 606–611.

Pinkel D, Segraves R, Sudar D, Clark S, Poole I, Kowbel D, Collins C, Kuo WL, Chen C, Zhai Y, Dairkee SH, Ljung BM, Gray JW and Albertson DG. (1998). *Nat Genet.*, **23,** 41–46.

Pinyol M, Hernandez L, Cazorla M, Balbín M, Jares P, Fernandez PL, Montserrat E, Cardesa A, Lopez-Otín C and Campo E. (1997). *Blood*, **89,** 272–280.

Rosenwald A, Wright G, Wiestner A, Chan WC, Connors JM, Campo E, Gascoyne RD, Grogan TM, Muller-Hermelink HK, Smeland EB, Chiorazzi M, Giltnane JM, Hurt EM, Zhao H, Averett L, Henrickson S, Yang L, Powell J, Wilson WH, Jaffe ES, Simon R, Klausner RD, Montserrat E, Bosch F, Greiner TC, Weisenburger DD, Sanger WG, Dave BJ, Lynch JC, Vose J, Armitage JO, Fisher RI, Miller TP, LeBlanc M, Ott G, Kvaloy S, Holte H, Delabie J and Staudt LM. (2003). *Cancer Cell*, **3,** 185–197.

Saltman DL, Cachia PG, Dewar AE, Ross FM, Krajewski AS, Ludlam C and Steel CM. (1988). *Blood*, **72,** 2026–2030.

Saxena A, Clark WC, Robertson JT, Ikejiri B, Oldfield EH and Ali IU. (1992). *Cancer Res.*, **52,** 6716–6721.

Schaffner C, Idler I, Stilgenbauer S, Dohner H and Lichter P. (2000). *Proc. Natl. Acad. Sci. USA*, **97,** 2773–2778.

Schultz DC, Vanderveer L, Berman DB, Hamilton TC, Wong AJ and Godwin AK. (1996). *Cancer Res.*, **56,** 1997–2002.

Seto M, Yamamoto K, Iida S, Akao Y, Utsumi KR, Kubonishi I, Miyoshi I, Ohtsuki T, Yawata Y, Namba M and Ueda R. (1992). *Oncogene*, **7,** 1401–1406.

Stilgenbauer S, Winkler D, Ott G, Schaffner C, Leupolt E, Bentz M, Moller P, Muller-Hermelink HK, James MR, Lichter P and Dohner H. (1999). *Blood*, **94,** 3262–3264.

Suzuki R, Kuroda H, Komatsu H, Hosokawa Y, Kagami Y, Ogura M, Nakamura S, Kodera Y, Morishima Y, Ueda R and Seto M. (1999). *Leukemia*, **13,** 1335–1342.

U M, Miyashita T, Shikama Y, Tadokoro K and Yamada M. (2001). *FEBS Lett.*, **509,** 135–141.

Zhang X, Karnan S, Tagawa H, Suzuki R, Morishima Y, Nakamura S and Seto M. (2004). *Cancer Science*, **95,** 809–814.

MAJOR ARTICLE

Differences between T Cell–Type and Natural Killer Cell–Type Chronic Active Epstein-Barr Virus Infection

Hiroshi Kimura,[1] Yo Hoshino,[1] Shinya Hara,[1] Naomi Sugaya,[1] Jun-ichi Kawada,[1] Yukiko Shibata,[1] Seiji Kojima,[1] Tetsuro Nagasaka,[2] Kiyotaka Kuzushima,[3] and Tsuneo Morishima[4,a]

Departments of [1]Pediatrics and [2]Clinical Pathology, Nagoya University Graduate School of Medicine, [3]Division of Immunology, Aichi Cancer Center Research Institute, and [4]Department of Nursing, Nagoya University School of Health Sciences, Nagoya, Japan

Infections of T cells and natural killer (NK) cells play a central role in the pathogenesis of chronic active Epstein-Barr virus (CAEBV) infection. To characterize the virologic and cytokine profiles of T cell–type and NK cell–type infection, 39 patients with CAEBV infection were analyzed. Patients with T cell–type infection had higher titers of immunoglobulin G against early and late EBV antigens, suggesting lytic cycle infection. However, the pattern of EBV gene expression was latency type II; *BZLF1*, which is a hallmark of lytic cycle infection, could not be detected in any patients, regardless of infection type. Patients with CAEBV infection had high concentrations of proinflammatory, T helper cell type 1, and anti-inflammatory cytokines. The cytokine profile in patients with NK cell–type infection was similar to that in patients with T cell–type infection, but the concentration of IL-13 was high in patients with NK cell–type infection. These findings should help to clarify the pathogenesis of CAEBV infection and facilitate the development of more-effective treatments.

Epstein-Barr virus (EBV) is a ubiquitous virus that infects most individuals by early adulthood. Primary EBV infection is usually asymptomatic but sometimes progresses to infectious mononucleosis, which resolves spontaneously after the emergence of EBV-specific immunity [1, 2]. EBV infection can be chronic in apparently immunocompetent hosts [3, 4]. Chronic active EBV (CAEBV) infection is characterized by chronic or recurrent mononucleosis-like infectious symptoms, such as fever, persistent hepatitis, extensive lymphadenopathy, hepatosplenomegaly, pancytopenia, uveitis, interstitial pneumonia, hydroa vacciniforme, and hypersensitivity to mosquito bites [3–5]. Patients with CAEBV infection have an unusual pattern of EBV-related antibodies and high viral loads in peripheral blood [3–7]. CAEBV infection is associated with high mortality and morbidity.

Recent studies have indicated that the clonal expansion of EBV-infected T cells and natural killer (NK) cells plays a central role in the pathogenesis of CAEBV infection [5, 8–11]. In a previous study, we found that patients with CAEBV infection fall into 2 clinically distinct groups, on the basis of whether the infected cells in their peripheral blood were mainly T cells or NK cells [5]. T cell–type infection is characterized by fever and high titers of EBV-related antibodies, whereas NK cell–type infection is characterized by hypersensitivity to mosquito bites and high titers of IgE. Furthermore, patients with T cell–type infection have significantly poorer outcomes [5, 12]. EBV-infected T cells might become activated and release inflammatory cytokines, such as interferon (IFN)–γ or tumor necrosis factor (TNF)–α, resulting in severe inflammation and fever [13, 14]. However, it is still not known why these 2 manifestations of the disease have different symptoms and courses.

The purpose of the present study was to gain a better

Received 4 May 2004; accepted 23 August 2004; electronically published 6 January 2005.

Financial support: Japan Society for the Promotion of Science (grant JSPS-RFTF97L00703); Japan Ministry of Education, Culture, Sports, Science and Technology (grant 13670793).

[a] Present affiliation: Department of Pediatrics, Graduate School of Medicine and Dentistry, Okayama University, Okayama, Japan.

Reprints or correspondence: Dr. Hiroshi Kimura, Dept. of Pediatrics, Nagoya University Graduate School of Medicine, 65 Tsurumai-cho, Showa-ku, Nagoya 466-8550, Japan (hkimura@med.nagoya-u.ac.jp).

The Journal of Infectious Diseases 2005; 191:531–9

0022-1899/2005/19104-0008$15.00

understanding the pathogenesis of CAEBV infection by characterizing the virologic profiles of T cell–type and NK cell–type infection and identifying the differences between them. We analyzed 20 patients with T cell–type infection and 19 patients with NK cell–type infection. The 2 types of CAEBV infection were compared in both virologic and immunologic analyses, including an analysis of cytokine profiles.

PATIENTS, MATERIALS, AND METHODS

Patients. Thirty-nine patients with CAEBV infection were enrolled in the present study. Informed consent was obtained from all of the patients or their parents. Of the 39 patients, 24 had been included in our previous study of the clinical characteristics of CAEBV infection [5]. All of the patients met the following diagnostic criteria [5]: (1) they had EBV-related illness or symptoms for >6 months (including fever, persistent hepatitis, extensive lymphadenopathy, hepatosplenomegaly, pancytopenia, uveitis, interstitial pneumonia, hydroa vacciniforme, or hypersensitivity to mosquito bites); (2) they had increased quantities of EBV in either affected tissue or peripheral blood (the quantity of EBV was defined as increased when ⩾1 of the following criteria was met: EBV DNA was detected in either affected tissue or peripheral blood by Southern-blot hybridization, EBV-encoded small RNA 1 [EBER-1]–positive cells were detected in either affected tissue or peripheral blood [15], or $>10^{2.5}$ copies/μg DNA was detected in peripheral-blood mononuclear cells [PBMCs] [15]); and (3) they did not manifest evidence of any previous immunologic abnormalities or of any other recent infection that might explain the condition (all of the patients examined were negative for antibody against HIV).

Cells. For the EBV gene-expression experiment, a lymphoblastoid cell line (LCL) that was transformed with B95-8 virus was used as a positive control, and BJAB, an EBV-negative B cell line, was used as a negative control.

Samples. Samples were collected at the time of diagnosis or before the administration of immunosuppressive therapy, such as chemotherapy or hematopoietic stem-cell transplantation. EDTA-treated peripheral blood collected from patients was centrifuged and separated into plasma and cell fractions; the cell fractions were separated into PBMCs on Ficoll-Paque density gradients (Pharmacia Biotech).

Titers of anti–EBV nuclear antigen (EBNA) antibodies were measured by use of an anticomplement immunofluorescence method. Titers of anti–viral capsid antigen (VCA) and anti–early antigen–diffuse restricted (EA-DR) IgG were measured by use of an immunofluorescence method. These titers were measured in all patients.

DNA was extracted from either 2×10^6 PBMCs or 200 μL of plasma by use of a QIAamp blood kit (Qiagen). To differentiate between free EBV DNA molecules and virions or nucleocapsids, selected plasma samples were examined for EBV content by digestion with deoxyribonuclease (RQ1 RNase-free DNase; Promega) for 30 min at 37°C [16, 17]. As controls, pGEM-BALF5, a control plasmid DNA containing an EBV target gene, and the supernatants of LCL and BJAB cultures were used. LCL was treated with *n*-butyrate and phorbol 12-myristate 13-asetate, to induce lytic cycle infection, and the culture supernatants were used as a control that contained enveloped virions.

For patients from whom fresh samples were available ($n = 19$), RNA was extracted from 2×10^6 PBMCs by use of an RNA extraction kit (QIAamp RNA Blood Mini Kit; Qiagen). cDNA was synthesized by use of Superscript reverse transcriptase II (Gibco Life Technology), as described elsewhere [18].

Determination of EBV-infected cells. To determine which cells were infected with EBV, PBMCs were fractionated into $CD3^+$, $CD4^+$, $CD8^+$, $CD16^+$, $CD19^+$, and $CD56^+$ cells by use of an immunobead method (DynaBeads; Dynal A/S) [5]. For some patients with T cell–type infection from whom a sufficient quantity of PBMCs was obtained, fractionation into $CD4^+$ and $CD8^+$ cells was also performed. The fractionated cells were analyzed by either quantitative polymerase chain reaction (PCR) or in situ hybridization with the EBER-1 probe [15]. Patients were defined as having T cell–type infection when $CD3^+$ cells either were the main cells giving a positive hybridization signal with EBER-1 or contained more EBV DNA than other cells in the blood sample [5]. Patients were defined as having NK cell–type infection when $CD16^+$ or $CD56^+$ cells were the main ones containing EBV [5]. Repeated tests were performed for some patients, and similar results were obtained; in the present study, representative results are shown.

For some patients, infected cells were identified in biopsied or autopsied tissues, such as lymph nodes, liver, and spleen. Double labeling by use of in situ hybridization with the EBER-1 probe and immunostaining with surface marker antibody were performed as described elsewhere [19].

Clonality of EBV. The clonality of EBV was determined by Southern blotting with a terminal-repeat probe, as described elsewhere [20, 21]. PBMC-extracted genomic DNA was digested with *Bam*HI, subjected to gel electrophoresis, transferred to a nylon membrane, hybridized with a ^{32}P-labeled *Xho*I fragment from the terminal region of EBV, and visualized by autoradiography.

Quantification of EBV DNA. Both PBMCs and plasma from all of the patients were assayed for viral load. A real-time quantitative PCR assay with a fluorogenic probe was performed as described elsewhere [15, 22]. As a positive standard for quantification, pGEM-BALF5 was used [15]. The quantity of EBV DNA was calculated as the number of copies per microgram or per milliliter of plasma.

Amplification of EBV-specific RNA transcripts by PCR. To detect latent gene expression (*EBNA1, EBNA2,* and *LMP1* [latent member protein]), nested PCR was performed essentially as described elsewhere [23]. For *EBNA1,* 3 different primer